Planetary and Space Science 254 (2024) 106010

Contents lists available at ScienceDirect

Planetary and Space Science

journal homepage: www.elsevier.com/locate/pss

Modeling the interstellar dust detections by DESTINY$^+$ I: Instrumental constraints and detectability of organic compounds

Harald Krüger [a,b,*], Peter Strub [a,c], Maximilian Sommer [c,d], Georg Moragas-Klostermeyer [c], Veerle J. Sterken [e], Nozair Khawaja [f,c], Mario Trieloff [g], Hiroshi Kimura [b], Takayuki Hirai [b], Masanori Kobayashi [b], Tomoko Arai [b], Jon Hillier [f], Jonas Simolka [c], Ralf Srama [c]

[a] MPI für Sonnensystemforschung, Göttingen, Germany
[b] Planetary Exploration Research Center, Chiba Institute of Technology, Narashino, Japan
[c] Institut für Raumfahrtsysteme, Universität Stuttgart, Germany
[d] University of Cambridge, UK
[e] ETH Zürich, Department of Physics, Zürich, Switzerland
[f] Institute of Geological Sciences, Freie Universität Berlin, Germany
[g] Institut für Geowissenschaften, Universität Heidelberg, Germany

ARTICLE INFO

Keywords:
Interstellar dust
DESTINY$^+$
DDA
DESTINY$^+$ dust analyzer
(3200) Phaethon

ABSTRACT

The DESTINY$^+$ spacecraft will be launched to the active asteroid (3200) Phaethon in 2025. The spacecraft will be equipped with the DESTINY$^+$ Dust Analyzer (DDA) which will be a time-of-flight impact ionization mass spectrometer. In addition to the composition of impacting dust particles, the instrument will measure the particle mass, velocity vector, and surface charge. Here, we study the detection conditions of DDA for interstellar dust during the DESTINY$^+$ mission. We use the interstellar dust module of the Interplanetary Meteoroid environment for EXploration model (IMEX Sterken et al., 2013; Strub et al., 2019) to simulate the flow of interstellar dust through the Solar System. Extending earlier work by Krüger et al. (2019b) we consider the entire DESTINY$^+$ mission, i.e. the Earth-orbiting phase of the spacecraft during the initial approximately 1.5 years after launch, the nominal interplanetary mission phase up to the Phaethon flyby, and a four-years mission extension beyond the Phaethon flyby. The latter may include additional asteroid flybys. For predicting dust fluxes and fluences we take into account a technical constraint for DDA not to point closer than 90° towards the Sun direction for health and safety reasons of the instrument and in order to avoid electrical noise generated by photoelectrons. For the Earth orbiting phase after launch of DESTINY$^+$ our simulations predict that up to 28 interstellar particles will be detectable with DDA in 2026. In the following years the interplanetary magnetic field changes to a focussing configuration for small ($\lesssim 0.1\,\mu m$) interstellar dust particles. This increases the total number of detectable particles to 50 during the interplanetary mission of DESTINY$^+$ in 2027. In 2028 and 2029/30 approximately 160 and 190 particles will be detectable, respectively, followed by about 500 in 2030/31. We also make predictions for the detectability of organic compounds contained in the interstellar particles which is a strong function of the particle impact speed onto the detector. While organic compounds will be measurable only in a negligible number of particles during the Earth orbiting and the nominal interplanetary mission phases, a few 10s of interstellar particle detections with measurable organic compounds are predicted for the extended mission from 2028 to 2031.

1. Introduction

In 2025 the Japanese Space Agency JAXA will launch the DESTINY$^+$ (Demonstration and Experiment of Space Technology for INterplanetary voYage Phaethon fLyby and dUst Science) spacecraft to the active Near-Earth asteroid (3200) Phaethon (Kawakatsu and Itawa, 2013; Arai et al., 2018; Ozaki et al., 2022), with a flyby at the asteroid planned for 2028. Although DESTINY$^+$ was initially designed as a technology demonstration mission for deep space exploration using solar electric propulsion, the spacecraft will be equipped with three scientific instruments: Two cameras (the Telescopic CAmera for Phaethon, TCAP, and the Multiband CAmera for Phaethon, MCAP; Ishibashi et al., 2024), as well as the DESTINY$^+$ Dust Analyzer (DDA, Kobayashi et al., 2018;

* Corresponding author at: MPI für Sonnensystemforschung, Göttingen, Germany.
E-mail address: krueger@mps.mpg.de (H. Krüger).

https://doi.org/10.1016/j.pss.2024.106010
Received 26 July 2024; Received in revised form 17 October 2024; Accepted 13 November 2024
Available online 22 November 2024

Simolka et al., 2024). The latter will be an upgrade of the Cosmic Dust Analyzer on board the Cassini spacecraft which very successfully investigated dust throughout the Saturnian system (Srama et al., 2011).

1.1. Dust at Phaethon

Phaethon is an extraordinary near-Earth asteroid with a diameter of approximately 5–6 km (Yoshida et al., 2023). Its perihelion distance is presently 0.14 AU with an orbital period of 1.433 yr. Around perihelion its surface temperature reaches more than 1000 K, thus becoming one of the hottest objects in the Solar System, even exceeding Mercury by far. Phaethon is the source of the Geminids (Ryabova et al., 2019), one of the most active meteor showers visible in the Earth's night sky. While parent bodies of meteor showers are mostly comets, Phaethon is an Apollo-type asteroid with a carbonaceous B-type reflectance spectrum, similar to aqueously altered CI/CM meteorites, and of hydrated minerals (Licandro et al., 2007). Recently Phaethon was attributed to the rare CY-type carbonaceous chondrites (MacLennan and Granvik, 2024).

Recurrent dust ejection and a dust tail at perihelion were reported for Phaethon (Jewitt et al., 2013; Li and Jewitt, 2013; Zubko and Wada, 2023), while electrostatic dust lofting (Kimura et al., 2022) and thermal mineral decomposition were suggested as mechanisms capable of triggering dust ejection (MacLennan and Granvik, 2024). However, recent observations showed that the tail at perihelion can be attributed to sodium emission rather than dust (Zhang et al., 2023). On the other hand, neither a coma nor a tail were observed around 1.0 AU (Hsieh and Jewitt, 2005; Ye et al., 2018; Kimura et al., 2019).

Visual images of the Geminids meteoroid stream very near to the Sun revealed that the core of the observable stream is offset radially outward from Phaethon's orbit (Battams et al., 2020). Dynamical modeling of the trail particles showed that this could be explained by a catastrophic event that affected Phaethon a few thousands years ago (Cukier and Szalay, 2023). The physical properties of Phaethon were summarized by Hanuš et al. (2016), however, the mechanisms driving its activity remain unknown.

The main scientific goal of DDA is to investigate the distribution and composition of dust released from Phaethon, during the flyby at the asteroid in 2028. In addition, during its Earth orbiting phase, the interplanetary voyage to Phaethon and during a possible mission extension after the flyby, there will be the opportunity to measure other populations of space dust as well. These include dust in the Earth–Moon system (Yang et al., 2022), interplanetary dust in the zodiacal dust complex (Grün et al., 1997; Krüger et al., 2019b), and finally interstellar dust. In this work we focus on the detection conditions of interstellar dust particles with DDA. A companion paper by Hunziker et al. (in prep.) describes the effects of the initial size distribution, and the dust optical properties on the simulation results.

1.2. Interstellar dust

The origin of interstellar dust particles is related to condensation in the outflows of evolved stars and stellar explosions, followed by injection into the interstellar medium (Tielens, 1998, 2012). Such particles initially carry the elemental and isotopic signatures of nucleosynthetic processes inherited from their host stars, which can be inferred from isotopically anomalous interstellar grains that survived in primitive meteorites from the interstellar cloud from which our Solar System formed 4.6 Gyr ago (Gail et al., 2009; Leitner et al., 2012; Zinner, 2014). During their residence time in the interstellar medium, these grains are exposed to ultraviolet irradiation, interstellar shock waves, and mutual collisions, leading to amorphization and partially grain destruction, particularly in the hot interstellar medium. On the other hand, recondensation and agglomeration may also take place in cold, dense molecular clouds (Tielens, 2005; Zhukovska et al., 2008). Such recondensed interstellar grains with average cosmic elemental and isotopic abundances dominate the interstellar dust population (Zhukovska et al., 2008), which seems to be supported by direct measurements of contemporary interstellar dust (Altobelli et al., 2016).

The interstellar dust particles are composed of minerals and organic compounds (e.g., Herbst and van Dishoeck, 2009; Jørgensen et al., 2020). The presence of organic refractory components in interstellar grains has been revealed by observations of near-infrared absorption bands (Sandford et al., 1991). It is believed that such compounds form on the surface of silicate grains as a result of ice accretion and subsequent ultraviolet irradiation (Greenberg, 1989). A model of interstellar dust with a silicate core and an organic refractory mantle can describe the wavelength dependence of interstellar extinction in diffuse clouds (Greenberg and Hage, 1990).

The elemental abundances of dust in our local interstellar environment (Local Interstellar Cloud, LIC) are consistent with core–mantle grains consisting of Mg-rich pyroxene and Mg-rich olivine with additional less abundant minerals in the core, and organic refractory compounds of C, N, and O in the mantle (Kimura et al., 2003). The mass of the organic refractory mantle is comparable to the mass of the silicate core.

Observations of the gaseous interstellar and circumstellar media revealed more than 150 different C-containing molecular species, approximately 50 of them contain 6 or more atoms (Herbst and van Dishoeck, 2009; Jørgensen et al., 2020). The majority of these compounds are believed to be formed on icy dust grains. The formation and evolution of interstellar complex organic molecules during the formation of stars and planets has recently been reviewed by Jørgensen et al. (2020) and Ceccarelli (2023). More recent observations with the James Webb Space Telescope (JWST) revealed even more complex molecular species (Rocha et al., 2023).

In our local environment, the Sun and the heliosphere are surrounded by the LIC of warm diffuse gas and dust where dust is assumed to contribute about 1% to the cloud mass (Mann, 2010; Kimura, 2015; Krüger et al., 2015). The Sun's motion with respect to this cloud causes an inflow of interstellar matter into the heliosphere (Frisch et al., 1999).

In situ measurements performed by dust instruments onboard spacecraft are now a state-of-the art method for measuring the physical properties of individual dust particles in space. Modern impact ionization dust analyzers allow us to study the mass, impact speed and direction, electrical charge as well as elemental and molecular composition of sub-micrometer to micrometer sized particles (Grün et al., 1992a,b; Kissel et al., 2003; Srama et al., 2004; Altobelli et al., 2016; Khawaja et al., 2023).

After initial predictions based on zodiacal light measurements in the 1970s (Bertaux and Blamont, 1976; May, 2007), the dust instruments on board the Ulysses and Galileo spacecraft showed that a collimated stream of interstellar dust passes through the Solar System due to the Sun's motion relative to the LIC (Grün et al., 1993; Baguhl et al., 1995). The measured heliocentric speed of the dust flow is approximately $26\,\mathrm{km\ s^{-1}}$ (Grün et al., 1994; Krüger et al., 2015) and its direction is compatible with the measured direction of the inflowing interstellar neutral helium gas (Baguhl et al., 1995; Witte, 2004; Strub et al., 2015; Swaczyna et al., 2023). Recent reviews about interstellar dust in the Solar System and beyond were published by Mann (2010), Sterken et al. (2019, 2022).

The Cosmic Dust Analyzer on board the Cassini spacecraft analyzed 36 submicrometer-sized interstellar dust particles in situ (Altobelli et al., 2016). The measurements are in agreement with Mg-rich particles of silicate and oxide composition, partly with Fe inclusions. Major rock-forming elements (Mg, Si, Fe, and Ca) are present in cosmic abundances, with only small grain-to-grain variations, but S and C are depleted. The interstellar particles in the solar neighborhood appear to be homogenized, likely by repeated processing in the interstellar medium.

The Stardust spacecraft performed two types of interstellar dust measurements while traveling to its main mission target comet 81P/Wild 2: (1) seven submicrometer-sized interstellar particles were

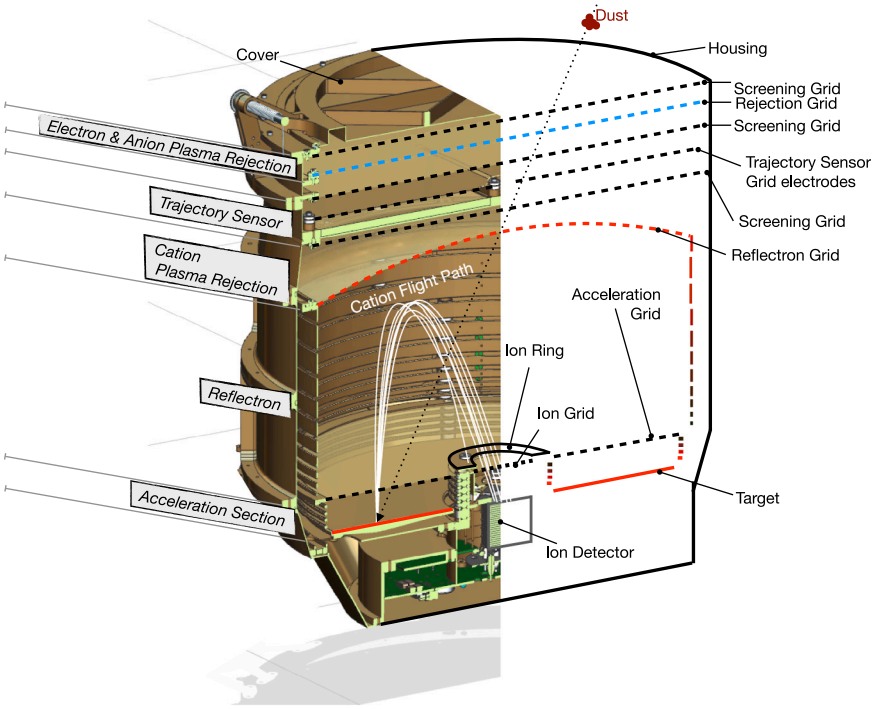

Fig. 1. Schematics of the DDA sensor head. Dust enters from the top. Structures drawn in black are electrically grounded. Blue color represents negative bias voltages, whereas red color stands for positive bias voltages. Measurements are taken at the trajectory sensor grid electrodes, ion ring, ion grid, target and ion detector (multiplier). On the left side of the figure, the flight path of the cations generated during a dust particle impact is illustrated.

successfully collected in a dedicated aerogel collector and returned to Earth (Westphal et al., 2014). The particles were diverse in elemental composition, crystal structure, and size. The presence of crystalline grains and multiple Fe-bearing phases, including sulfide, in some particles indicates that individual interstellar particles diverge from any one representative model of interstellar dust inferred from astronomical observations and theory. (2) Stardust also carried the Cometary and Interstellar Dust Analyzer (CIDA) on board which was an impact-ionization time-of-flight mass spectrometer (Kissel et al., 2003). The spectra of 45 presumably interstellar particles analyzed by CIDA during the spacecraft's interplanetary cruise, showed the presence of high mass organics (most probably aromatics together with O- and N- bearing moieties), without any certainty on the composition of the organic component (Krueger et al., 2004; Kissel et al., 2004). The authors did not describe the reasoning why they believe that these are interstellar rather than at least in part interplanetary particles, so their origin remains somewhat elusive.

Although these results by Cassini and Stardust opened a new window for a better understanding of the processes in the LIC, many open questions remain which will be addressed by DDA with its highly improved measurement capabilities as compared to earlier dust instruments (cf. Section 2 and Simolka et al. (2024)). These are the compositional diversity of the particles in the LIC, the inventory of organic compounds and the significance of dust processing in the interstellar medium, just to name a few, see also Section 5.

One particular aspect addressed in this paper is the organic component of the interstellar particles. A much better particle detection statistics together with measurements over a wide range of impact speeds in combination with the significantly higher mass resolution of DDA will very likely give an improved knowledge about the inventory of organic particle constituents. This will lead to a better understanding of the chemical processing of the grain constituents.

In addition to dust released from Phaethon – to be measured during the flyby of DESTINY$^+$ at the asteroid in 2028 – the in situ analysis of interstellar dust particles is one of the major scientific drivers for the DDA measurements. The interstellar dust flux in the inner Solar System is time-dependent on a 22-year timescale due to the particles' interaction with the time-varying interplanetary magnetic field (e.g. Landgraf et al., 2003; Sterken et al., 2013). Therefore, the interstellar dust flux is predicted to reach a maximum in the early 2030s (Strub et al., 2019). Given our expectation that the proposed DESTINY$^+$ extended mission will still be active at that time, in this paper we study the detection conditions for interstellar dust beyond the Phaethon flyby. A companion paper (Hunziker et al. in preparation) describes the modeling results for interstellar dust, using two different calibration methods and various material assumptions, and includes a discussion on the heliosheath filtering.

Krüger et al. (2019b) performed an initial analysis of the detection conditions of interplanetary and interstellar dust by DDA. In that work we focussed on the interplanetary mission phase of DESTINY$^+$, employing the planned spacecraft trajectory and DDA design available at the time. In that scenario the launch of the spacecraft was planned for 2022 with a Phaethon flyby scheduled for August 2026, and two DDA sensor heads with a total sensitive area of $0.035\,\mathrm{m}^2$ were foreseen. In the meantime, the launch was shifted to 2025 with a Phaethon flyby in January 2028, and the DDA instrument was reduced to one sensor head with a total sensitive area of $0.03\,\mathrm{m}^2$ (Fig. 1). In addition, there have been considerations for a mission extension into the 2030s by JAXA, with additional asteroid flybys if spacecraft health allows.

Here we update and extend our earlier investigation of the DDA dust detection conditions published by Krüger et al. (2019b). In addition to using an updated DESTINY$^+$ trajectory and DDA sensor profile, we now include the early mission phase after launch when DESTINY$^+$ will still be orbiting the Earth, and we study a mission extension beyond Phaethon flyby until 2032. Furthermore, we take an instrumental constraint into account which implies that DDA should not point closer than 90° towards the Sun for health and safety reasons and to avoid instrumental noise. Finally, we evaluate the detectability of organic matter in the interstellar particles which is significantly affected by the particle impact speed (Khawaja et al., 2019, 2023). Dust at Phaethon

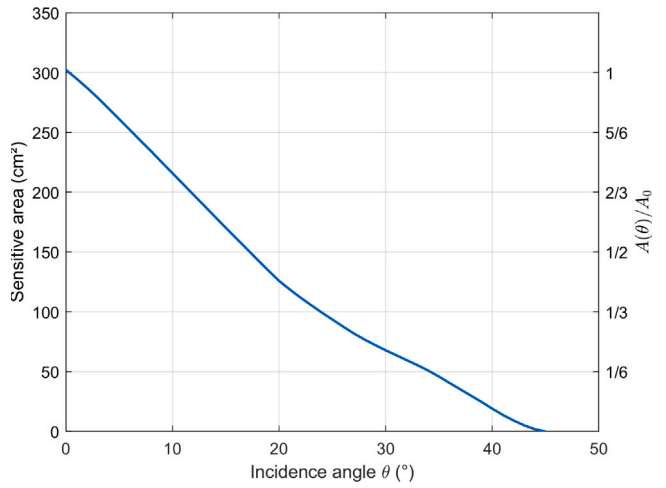

Fig. 2. The effective sensitive area of DDA as a function of incidence angle θ.

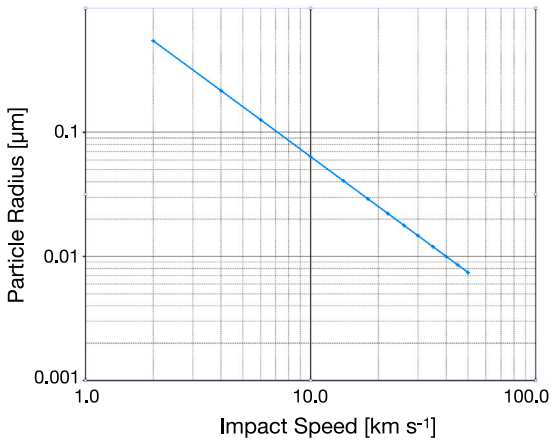

Fig. 3. Minimum detectable particle size (detection threshold) of DDA for silicate particles (density $\rho = 3000$ kg m^{-3}) as a function of particle impact speed v onto the sensor target.

was studied by Szalay et al. (2019), and for the detection conditions of interplanetary dust we refer the reader to our earlier paper (Krüger et al., 2019b).

2. DESTINY$^+$ Dust Analyzer

The DESTINY$^+$ Dust Analyzer (DDA) is an impact ionization dust analyzer dedicated to performing in situ measurements of individual micrometer and sub-micrometer sized dust particles (Figure 1; Simolka et al., 2024). It has evolved from the dust analyzers previously flown on board the Giotto, Stardust and Cassini spacecraft (Kissel, 1986; Kissel et al., 2003; Srama et al., 2004). DDA will be equipped with a two-axes pointing mechanism which can turn the instrument by 90° in elevation and 180° in azimuth, respectively. The pointing mechanism allows us to scan the sky and point the sensor aperture in the direction of the dust flow so that it can be operated like a dust telescope (Simolka et al., 2024). The dust sensor including the pointing mechanism are mounted on the exterior of the DESTINY$^+$ spacecraft.

In addition to the composition of impacting dust particles, the instrument will measure the particle mass, velocity vector, and surface charge. For measurements with a sufficiently large signal-to-noise ratio, the velocity vector will be determined with an accuracy of approximately 10% for the speed and with an angular accuracy of about 10°. The particle mass can be determined with an accuracy of better than a factor of ten. This will allow us to constrain the trajectory, and thus the source population, of each detected particle individually (Hillier et al., 2007).

The sensor head consists of a cylindrical housing with an aperture of 287 mm in diameter (cf. Fig. 1). A door cover protects the interior of the sensor head from contamination during ground handling activities and during launch. The cover will be opened approximately six to eight weeks after launch. Inside the housing there are a series of functional modules for measuring incoming dust particles: (i) the rejection module, (ii) trajectory sensor, and (iii) a mass spectrometer. The key elements of the DDA mass spectrometer are the impact target covered with a 25 µm thick gold surface layer, the acceleration stage, reflectron and ion measurement module. The positively charged ions released during the particle impact at the target are measured with an electron multiplier (Simolka et al., 2024). The setup is illustrated in Fig. 1.

Taking into account all grids at the sensor entrance, the effective total sensitive area for normal incidence is 0.03 m^2. The sensitive area gradually decreases with increasing incidence angle, and reaches zero at a maximum incidence angle of approximately 45° (Fig. 2). Dust analyzers similar to the DDA instrument are also under development for the Interstellar Mapping and Acceleration Probe (IMAP) and the Europa Clipper missions, respectively (Sternovsky et al., 2022; Goode et al., 2023).

In the atomic mass range of 1 to 100 u, the mass resolution $m/\Delta m$ is sufficient to resolve individual ion species, i.e. $\Delta m < 1$ u (Simolka et al., 2024). A mass spectrum covers a mass range between 1 and 1000 u which allows for the detection of high mass organics as well as molecular fragments and clusters.

The detection threshold of impact ionization dust sensors is a strong function of the particle impact speed (Göller and Grün, 1989). For DDA this is shown in Fig. 3 which shows the minimum detectable particle size for varying impact speeds. For example, at 10 km s^{-1} the smallest detectable particles are expected to be approximately 0.05 µm in radius.

Based on the sensor design, the DDA instrument shall not measure during direct Sun exposure. Given that the instrument's electron multiplier faces towards open space, solar illumination of the inner sensor may lead to multiplier degradation. Furthermore, given that target cleanliness is critical for the DDA measurements, heating of the sensor target due to solar illumination may lead to the formation of complex organic target contamination from more simple compounds present even after the most intense target cleaning before launch. Finally, photoelectrons released from the inner sensor wall may lead to strong electrical noise. Elevated noise rates were registered, for example, by the dust detectors on board the Ulysses and Nozomi spacecraft when the Sun illuminated the inner sensor walls (Baguhl et al., 1993; Senger, 2007). These requirements imply that the sensor shall not point closer than 90° towards the Sun direction (in the following called DDA Sun avoidance constraint).

3. Interstellar dust simulations

Similar to our earlier paper (Krüger et al., 2019b), we use the Interplanetary Meteoroid environment for EXploration (IMEX) interstellar dust model developed by Sterken et al. (2012, 2013) and Strub et al. (2019) to simulate the flow of interstellar dust through the Solar System. The model takes into account solar gravity, solar radiation pressure and the electromagnetic interaction with the interplanetary magnetic field. To describe the detection geometry, we use an updated DDA sensor profile with one DDA sensor head and a total sensor area of 0.03 m^2 (Figure 1; Kobayashi et al., 2018; Simolka et al., 2024). Based on these assumptions we derive dust fluxes and fluences during various mission phases defined in Section 3.1. All dust impact directions, impact speeds, and dust fluxes/fluences are given in a spacecraft-fixed reference frame. We take into account a DDA pointing constraint which

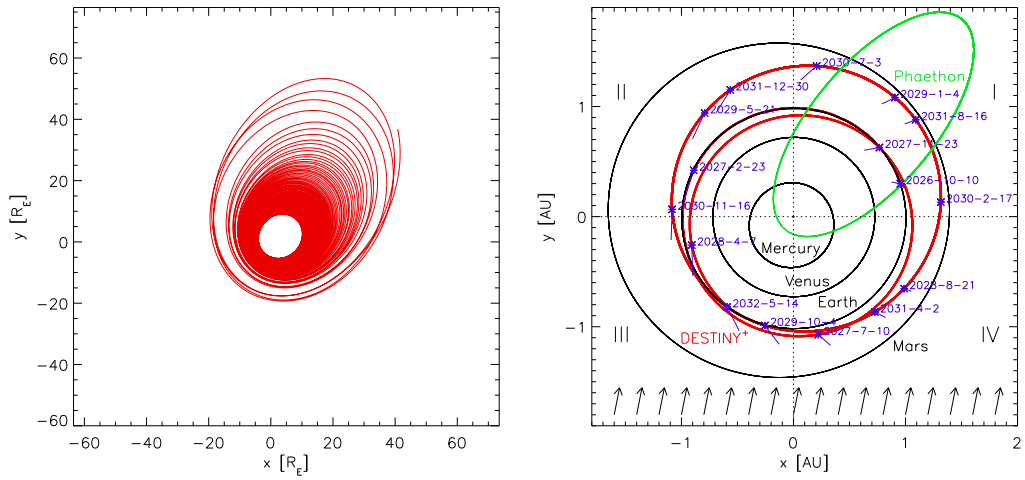

Fig. 4. *Left:* Trajectory of DESTINY⁺ during its Earth orbiting phase between 12 November 2025 and 16 December 2026 (Earth radius R_E = 6378.1 km). *Right:* Interplanetary trajectories of DESTINY⁺ from 10 October 2026 to 16 May 2032 (red) and (3200) Phaethon (green) projected onto the ecliptic plane. Black arrows at the bottom indicate the flow of interstellar dust particles with a ratio of solar radiation pressure over gravity $\beta = 1$, assumed to be co-aligned with the flow of interstellar neutral helium (Witte et al., 2004; Wood et al., 2015). The impact directions of these particles in the spacecraft-fixed coordinate system at selected times are indicated by blue lines where the line length is proportional to the particle impact speed. Vernal equinox is to the right. DESTINY⁺ trajectory from JAXA/ISAS, see text for details.

implies that for health and safety reasons and to avoid noise events, the DDA instrument shall not measure during direct Sun exposure and thus the sensor shall not point closer than 90° towards the Sun direction (see Section 3.2). Finally, for our dust modeling we assume that the DDA sensor always points into the direction of the interstellar dust flow averaged over all simulated particle sizes. This is necessary because the flow directions of the different particle sizes typically differ by 20-30° in periods when the dust flux is high.

3.1. DESTINY⁺ Mission Phases and Trajectory

The DESTINY⁺ trajectory is shown in Fig. 4. For our simulations we distinguish three mission phases:

(1) An early phase when the spacecraft is on a spiraling orbit around the Earth. This phase lasts from launch in 2025 until approximately the first lunar flyby in late 2026. The presently available DESTINY⁺ trajectory for this mission phase covers the time interval from 12 November 2025 to 16 December 2026.
(2) The lunar flyby phase and the nominal interplanetary mission. Trajectory data are available from 10 October 2026. In our scenario this phase ends in January 2028 after the flyby at the asteroid Phaethon.[1]
(3) An extended mission which begins in January 2028 after the Phaethon flyby.[1] Trajectory data are available until 16 May 2032.

For our simulations we use sample trajectories for DESTINY⁺ provided by JAXA/ISAS for study purposes. They are available as supplementary online material. The final spacecraft trajectory will depend on the exact launch date of DESTINY⁺ among other factors and will very likely be different. Given that DESTINY⁺ will stay in a heliocentric distance range close to 1 AU during its entire mission, the effect of a trajectory update for our simulation results for interstellar dust is expected to be minor, in particular smaller than the uncertainties of our simulation results, see Section 5.

[1] JAXA considers the time period until May 2028 as the nominal mission, while for our simulations we assume that it ends in January 2028 with the flyby at Phaethon for simplicity.

3.2. DDA Sun avoidance constraint

As described in Section 2 the sensor shall not point closer than 90° towards the Sun direction (DDA Sun avoidance constraint). Therefore, for our dust simulations we have to determine the time intervals when the angle between the average interstellar dust impact direction (averaged over all sizes) and the Sun direction (dust–spacecraft–Sun angle measured in the spacecraft-based reference frame) is larger than 90°. To this end, we assume that the interstellar dust inflow is co-aligned with the direction of the interstellar neutral helium gas flow into the Solar System (Witte et al., 1996; Lallement and Bertaux, 2014; Wood et al., 2015; Swaczyna et al., 2023), in the following called nominal interstellar dust direction. For the inflowing dust particles this means that the ratio of solar radiation pressure over gravity is assumed to be $\beta = 1$. This approximation is strictly valid only for a limited particle size of approximately 0.3–0.5 μm radius (Kimura et al., 2003; Kimura, 2017). Larger and smaller particles with other β values approach the spacecraft from somewhat different directions. Thus, strictly, the time when the dust–spacecraft–Sun angle reaches 90° depends on the particle size. Nevertheless, we calculate the Sun avoidance constraint as the time when $\beta = 1$ particles reach a dust–spacecraft–Sun angle of 90° for simplicity.

Throughout this paper we take the DDA Sun avoidance constraint into account. Any additional constraints potentially restricting the sensor pointing like, e.g., the spacecraft orientation or shielding by the Earth, are not considered. They are beyond the scope of this paper. Similarly, gravitational focussing by the Earth, which may affect both the dust approach directions and the fluxes, is not taken into account in the IMEX interstellar dust model.

3.3. Interstellar dust model

The IMEX model uses the same initial conditions as Landgraf (2000) and Sterken et al. (2012, 2013): Dust particles immersed in the LIC, through which the Solar System currently passes, penetrate the planetary system (Grün et al., 1994; Mann, 2010; Krüger et al., 2019a; Sterken et al., 2019, and references therein). The interstellar particles enter the heliosphere from the Sun's apex direction with the speed of the Sun relative to the local interstellar cloud (26 km s^{-1}), and an inflow direction from an ecliptic longitude l_{ecl} = 259° and latitude b_{ecl} =

8° (Witte et al., 1996; Frisch et al., 1999).[2] Typically, interstellar dust moves through the Solar System on unbound, hyperbolic trajectories. Within the measurement accuracy, the dust inflow direction is the same as the direction of the neutral interstellar helium gas inflow into the Solar System (Grün et al., 2001; Witte, 2004; Lallement and Bertaux, 2014; Wood et al., 2015; Strub et al., 2015; Swaczyna et al., 2023). This is equivalent to the interstellar particles being at rest with respect to the LIC.

Strub et al. (2019) performed simulations of interstellar dust particles near Earth orbit using the IMEX model. The IMEX model simulates the dynamics of charged micrometer and sub-micrometer sized interstellar particles taking into account solar gravity, solar radiation pressure, and the electromagnetic interaction due to a time-varying interplanetary magnetic field. In contrast to interplanetary dust, the predicted impact speeds and fluxes of the interstellar particles at the Earth exhibit strong variations due to the motion of the Earth around the Sun. Their impact speeds and fluxes near Earth orbit become maximal in spring when the Earth moves head-on to the interstellar dust stream, thus leading to maximum impact speeds exceeding $60\,\mathrm{km\ s^{-1}}$ while in autumn the impact speeds are below $20\,\mathrm{km\ s^{-1}}$ (Strub et al., 2019, see also Figures 7 and 11). Given that the trajectories of the interstellar particles are affected by solar radiation pressure and the solar magnetic field, the impact speeds and fluxes are also modulated by the solar activity. Such modulations will be detectable by DDA because DESTINY$^+$ will move around the Sun on a nearly circular trajectory at approximately 1 AU (Fig. 4, right panel).

The IMEX interstellar dust model simulates the dynamics of particles in the size range from 0.05 μm to 5 μm in 12 size bins. The dynamics of each of these sizes was simulated individually, assuming the adapted β curve for astronomical silicates (Sterken et al., 2012). In the IMEX model, the dust density in the Solar System is calibrated with the Ulysses interstellar dust measurements, again individually for each size bin (Strub et al., 2019). Due to the variable interplanetary magnetic field (IMF), the model is time-dependent. A detailed description of the forces acting on the particles and the resulting general interstellar dust flow characteristics was given by Sterken et al. (2012). A comparison of the IMEX model predictions with the interstellar dust measurements of other spacecraft (Helios, Galileo, Cassini) was performed by Krüger et al. (2019a), while a detailed comparison with the Ulysses data was made by Landgraf et al. (2003) and Sterken et al. (2015).

The IMF shows systematic variations with time, including the 25-day solar rotation and the 22-year solar magnetic cycle, as well as local deviations caused by disturbances in the interplanetary magnetic field, due to, e.g. Coronal Mass Ejections (CMEs) and Corotational Interaction Regions (CIRs). The dust particles in interplanetary space are typically charged to an equilibrium potential of +5 V (Mukai, 1981; Horányi, 1996; Kimura and Mann, 1998; Kempf et al., 2004). Small or more porous particles have a higher charge-to-mass ratio, hence their dynamics is more sensitive to the interplanetary magnetic field. The major effect of the magnetic field on the charged interstellar dust is a focussing and defocussing relative to the solar equatorial plane with the 22-year magnetic cycle of the Sun (Gustafson and Lederer, 1996; Landgraf, 2000; Landgraf et al., 2003; Sterken et al., 2012, 2013). Modifications of the particle dynamics by solar radiation pressure and the Lorentz force acting on charged dust particles have to be taken into account for a proper interpolation of the interstellar dust properties to the interstellar medium outside the heliosphere where these particles originate from (Slavin et al., 2012; Sterken et al., 2013). In particular, strong filtration of small grains due to electromagnetic forces occurs at the heliospheric boundary, leading to a strong modification of the size distribution and fluxes of grains measured inside the heliosphere (Linde and Gombosi, 2000; Slavin et al., 2012; Godenko and Izmodenov, 2024).

Statistical errors affect the modeling in two different ways: first, the error from the statistical limitations of the Monte Carlo simulation itself, which can be maintained by the trade-off between computation time and the Poisson error of the number of test particles passing through the cells of the simulation data cube. The number of test particles was chosen such that this error is $\lesssim 10\%$. Second, there is a statistical error in the normalization of the particle densities due to the limited number of particles available in the Ulysses dataset used for calibration.

With a total of about 600 measured particles used to determine the normalization of 10 size bins, and the number of particles distributed unevenly with the particle count per bin increasing towards smaller sizes, the statistical error can reach up to 30%, with only 10 particles in the largest size bin used in this simulation (1 μm).

These uncertainties mostly affect the density and flux. The velocity and directionality of the particles are much better constrained, as these quantities are essentially determined by the particle position relative to the Sun. They vary only slightly throughout a cell in the data cube.

The testing of the model predictions is hampered by the scarcity of observations of the interstellar dust flow through the Solar System. To this date, 15 years after the mission's end, the Ulysses dataset is still the most comprehensive dataset of interstellar dust in the Solar System available. Due to this, the IMEX model still represents the current understanding of interstellar dust in the Solar System, and implements the β curve that is the best fit for the Ulysses dataset. A parameter study of different materials and a variety of β curves using the same simulation code is currently underway (S. Hunziker et al. in preparation).

The largest uncertainties, however, are not statistical in nature, they rather are due to uncertainties in the material properties of the dust particles (composition, porosity, β), and for the smallest particles, interactions with random outflows of solar material, such as CMEs and CIRs (Flandes et al., 2011; Baalmann et al., 2024).

In this work, the dust particles are assumed to be astronomical silicates (Draine and Lee, 1984), but scaled to match the radiation pressure factor $\beta = 1.6$ suggested by Landgraf et al. (1999), based on measurements by Galileo and Ulysses. The authors also argue that particles with $\beta \gtrsim 2$ are incompatible with the observed dynamics. Carbonaceous particles can have maximum β values in the range of 1–2 or even higher depending on particle porosity, while the maximum β values of pure silicate particles do not exceed unity (Kimura and Mann, 1999). Thus, the β values derived by Landgraf et al. (1999) are in agreement with carbonaceous particles rather than silicate particles, while the interstellar particles identified in the Stardust sample and the ones analyzed with Cassini/CDA are mostly composed of silicates (Westphal et al., 2014; Altobelli et al., 2016). Interstellar carbon particles have not been identified in any in situ dataset yet, and while a minor contribution cannot be ruled out, they likely do not play a major role in the overall picture of interstellar dust in the Solar System.

Ongoing work by Hunziker et al. (priv. comm.) uses the same interstellar dust simulation code to examine a broader range of material parameters of β and particle size. Preliminary results indicate that the flux predictions depend on the choice of β curve, i.e. the choice of material and porosity. Within a range of parameters compatible with previous work (i.e. no significant contribution of carbon, $\beta < 2$), the flux predictions using different β curves are within a factor of 2 or less of the baseline simulation presented in this work.

This factor of two uncertainty is in agreement with the empirical estimate of the model uncertainty of a factor of 2–3 derived in Krüger et al. (2019a). In that work, the authors compared the flux predictions

[2] Recently, the inflow vector of the interstellar neutral helium was determined at $l_{\mathrm{ecl}} = 255.73° \pm 0.19°$, $b_{\mathrm{ecl}} = 5.04° \pm 0.15°$, speed $v = 26.63 \pm 0.17\,\mathrm{km\ s^{-1}}$ (Swaczyna et al., 2023), i.e. an offset of 4.44° relative to the direction assumed in our simulations (Strub et al., 2019). Taking into account DDA's opening angle of approximately 45°, and its sensitivity profile (Fig. 2), this leads to uncertainties $\lesssim 10\%$ and can be neglected given the overall uncertainties in the dust measurements and the width of the simulated ISD stream of 10–20° (Strub et al., 2019).

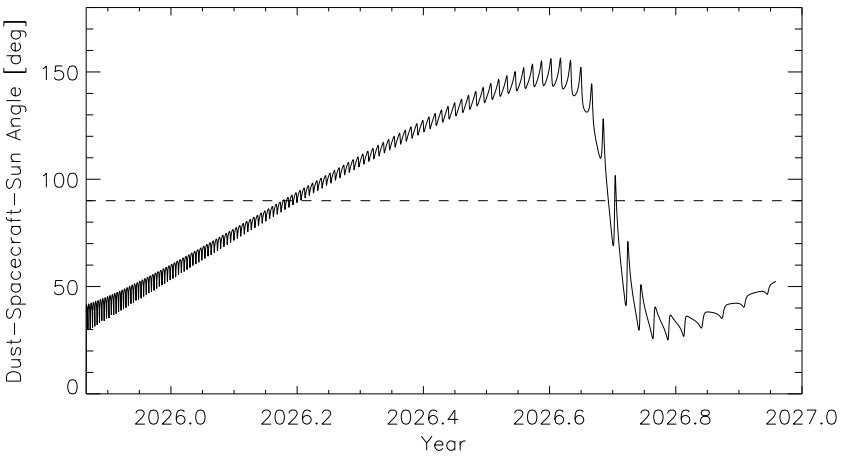

Fig. 5. Angle between the nominal interstellar dust direction and the direction towards the Sun in the spacecraft-centered reference frame during the Earth orbiting phase of DESTINY⁺. Interstellar dust will not be measurable during the intervals when the angle is below 90° due to the DDA Sun avoidance constraint.

of the IMEX model with in situ observations of the interstellar dust flow by four different missions, namely Helios, Galileo, Ulysses, and Cassini, and concluded that the model's predictions were within a factor of 2–3 of the observed fluxes. In order to improve on this, a much higher number of interstellar particle detections is needed, e.g. using a new generation large area dust detector on a long-term mission, and an improved understanding of the composition of the interstellar particles flowing through the Solar System.

As discussed earlier and shown in Fig. 3, the detection threshold for $10\,\mathrm{km\ s^{-1}}$ impact speed is approximately $0.05\ \mu\mathrm{m}$ and this implies a mass threshold of 10^{-19} kg which we use for our interstellar dust simulations. Given that the impact speeds of interstellar particles onto DDA are usually much higher than $10\,\mathrm{km\ s^{-1}}$, during long time periods the instrument will likely be able to detect even smaller particles than those covered by our simulations (cf. Section 4), if they are able to pass through the heliospheric boundary regions. For more details of the model and its earlier application to DESTINY⁺ the reader is referred to Strub et al. (2019) and Krüger et al. (2019b).

4. Results

In this Section we present our simulation results for the DESTINY⁺ mission phases described in Section 3.1.

4.1. Earth orbiting phase

The DESTINY⁺ trajectory during the Earth orbiting phase is shown in the left panel of Fig. 4. Presently, trajectory data for this phase are available from 11 November 2025 to 16 December 2026.

Early in the mission during the first few months after launch, the orbital period of DESTINY⁺ will be only a few hours. Tests of the spacecraft and the instruments will be performed during this mission phase, and passages through the Earth's radiation belts will occur twice per spacecraft orbit, among other restrictions resulting in a reduced DDA measurement time. No dedicated interstellar dust measurements are presently foreseen for this early phase.

During the Earth orbiting phase the DESTINY⁺ orbit will be gradually raised by the ion engines of the spacecraft, leading to a slowly increasing orbital period. There will be two dynamical factors affecting the dust particles' velocity vector, i.e. the particle impact speed and direction, in the spacecraft-centered reference frame: (1) The motion of DESTINY⁺ around the Earth will lead to a modulation of the interstellar dust flow vector during each spacecraft orbit and (2) There will be an annual modulation caused by the Earth's motion around the Sun.

Fig. 5 shows the angle between the nominal interstellar dust direction and the direction towards the Sun (dust–spacecraft–Sun angle) in the spacecraft-centered reference frame. Interstellar particles can only be measured if this angle is larger than 90°, i.e. above the dashed line (cf. Section 3.2). This is the case roughly between mid March and mid August 2026. The Sun avoidance constraint excludes approximately 50% of the total time in this mission phase from interstellar dust measurements. The superimposed sawtooth pattern is due to the variation of the interstellar dust direction in the spacecraft-centered reference frame during one spacecraft orbit around the Earth.

In Fig. 6 we show the simulated dust fluxes for all relevant particle sizes. Dashed areas indicate the time intervals when interstellar dust will not be measurable. Our simulations predict that no particles in the size bins $0.16\ \mu\mathrm{m}$ and $0.23\ \mu\mathrm{m}$ will be detectable because they are strongly affected by the solar radiation pressure and thus prevented from entering the inner Solar System (e.g., Sterken et al., 2013; Strub et al., 2019). The sawtooth pattern, which is particularly evident in the bottom panel showing the flux added together for all particle sizes, is again due to the spacecraft motion around the Earth.

For the smallest particles ($0.05\ \mu\mathrm{m}$ and $0.07\ \mu\mathrm{m}$, top panels in Fig. 6) the time intervals with rather high predicted fluxes partially coincide with the time period when interstellar dust will be undetectable due to the DDA Sun avoidance constraint. Here, the predicted dust fluxes are high because the spacecraft and the dust approximately move in opposite directions, leading to high dust impact speeds. However, the flux maxima are predicted for the first half of the interval when DDA will be allowed to point into the interstellar dust flow, i.e. from approximately mid March until end of June 2026. Fig. 7 shows the particle impact speeds and impact direction (averaged over all sizes) together with the fluxes for three selected particle sizes. For all these sizes the expected impact speeds are rather high in the range of 40 to $60\,\mathrm{km\ s^{-1}}$ during the time interval when interstellar dust will be detectable.

For the intermediate size ($0.11\ \mu\mathrm{m}$ and $0.34\ \mu\mathrm{m}$) particles the situation is similar. The highest fluxes are also expected from approximately March to May 2026, but with somewhat lower impact speeds between 40 and $50\,\mathrm{km\ s^{-1}}$. For the biggest particles ($0.49\ \mu\mathrm{m}$ and $0.72\ \mu\mathrm{m}$) the situation is different. Here the flux peaks occur when the Earth is in the downstream region of the interstellar dust behind the Sun with respect to the incoming direction of the interstellar dust flow. Unfortunately, the DDA Sun avoidance constraint largely excludes this region from interstellar dust measurements.

Finally, the fluences for individual particle sizes are displayed as a histogram in Fig. 8 and summarized in Table 1. Our simulations predict that 28 particles will be detectable between 14 March and 10 September 2026. Six of these particles are in the size range of approximately 0.3 to $0.5\,\mu\mathrm{m}$ radius, the rest having radii of $0.1\,\mu\mathrm{m}$ or less. Note that these are optimistic numbers that neither take constraints by spacecraft operations into account nor times when the Earth may be in the DDA field of view.

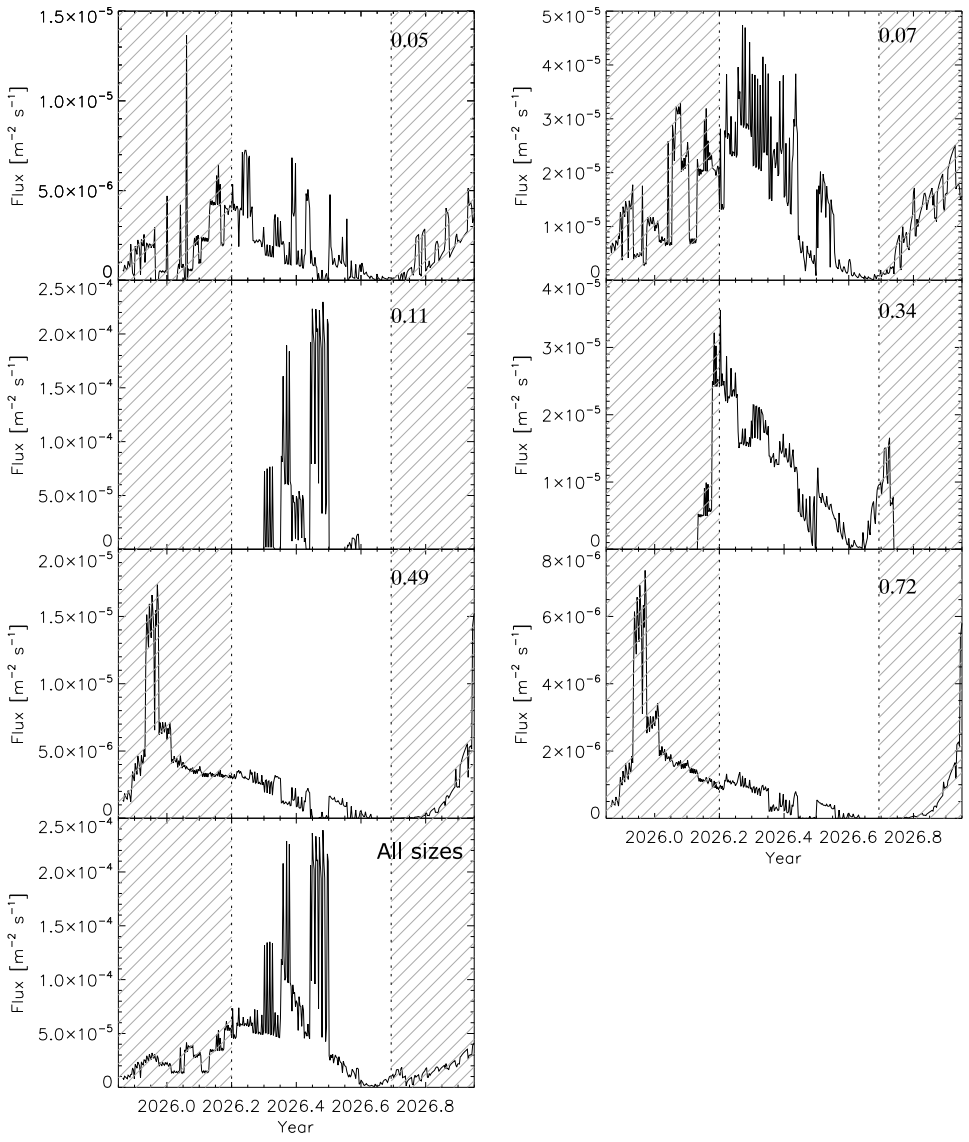

Fig. 6. Dust fluxes for the Earth orbiting phase of DESTINY$^+$ for all relevant particle sizes individually (top three rows) and for all sizes added together (bottom panel). The forbidden time intervals due to the DDA Sun avoidance constraint are indicated by the dashed areas. The time resolution along the spacecraft trajectory is 1/20 day. The numbers at the top right in each panel give the particle radius in micrometers.

4.2. Interplanetary mission

4.2.1. Nominal mission

For the interplanetary mission phase of DESTINY$^+$ the interstellar dust direction is illustrated in the right panel of Fig. 4: Only in the bottom part of the Figure in quadrants III and IV will the dust–spacecraft–Sun angle become larger than 90° for most of the time. Here, interstellar dust will be measurable. On the contrary, interstellar dust will be undetectable in most of quadrants I and II.

Our simulations for this mission phase start on 10 October 2026. DESTINY$^+$ will leave the Earth's orbit in April 2027 after two consecutive gravitational swingbys at the Moon. The flyby at Phaethon is scheduled for January 2028, and additional asteroid flybys may occur later during an optional mission extension (see Section 4.2.2).

In Fig. 9 we show the dust–spacecraft–Sun angle for the DESTINY$^+$ interplanetary mission. As before, interstellar dust can be measured above the dashed line when this angle is larger than 90°. Similar to the Earth orbiting phase, interstellar dust can be measured during only approximately half of the mission time, and the time intervals allowed for interstellar dust detection are again listed in Table 1.

In Fig. 10 we show our simulated dust fluxes for all relevant particle sizes for the entire interplanetary mission, and Fig. 11 shows the particle impact speeds and impact direction together with the fluxes for three selected particle sizes. All quantities are an average over all particles in each cubic grid cell of 0.25 AU side length. In general, the situation is similar to the one in the Earth orbiting phase (Section 4.1). For the smallest particles (0.05 μm and 0.07 μm, top panels in Fig. 10) the flux peaks partially fall in the time interval when interstellar dust will be undetectable due to the DDA Sun avoidance constraint. The highest flux typically occurs within the first half of the allowed intervals when the expected impact speeds are in the range of 40 to 60 km s^{-1}.

For the intermediate size particles the situation is also similar to the Earth orbiting phase: The highest fluxes are again expected during approximately the first half of the allowed time interval, although with somewhat lower impact speeds between 30 and 50 km s^{-1}. For the biggest particles the flux peaks occur when the spacecraft is in the downstream region of the interstellar dust behind the Sun with respect to the incoming interstellar dust flow. This region is largely excluded from interstellar dust measurements due to the DDA Sun avoidance constraint.

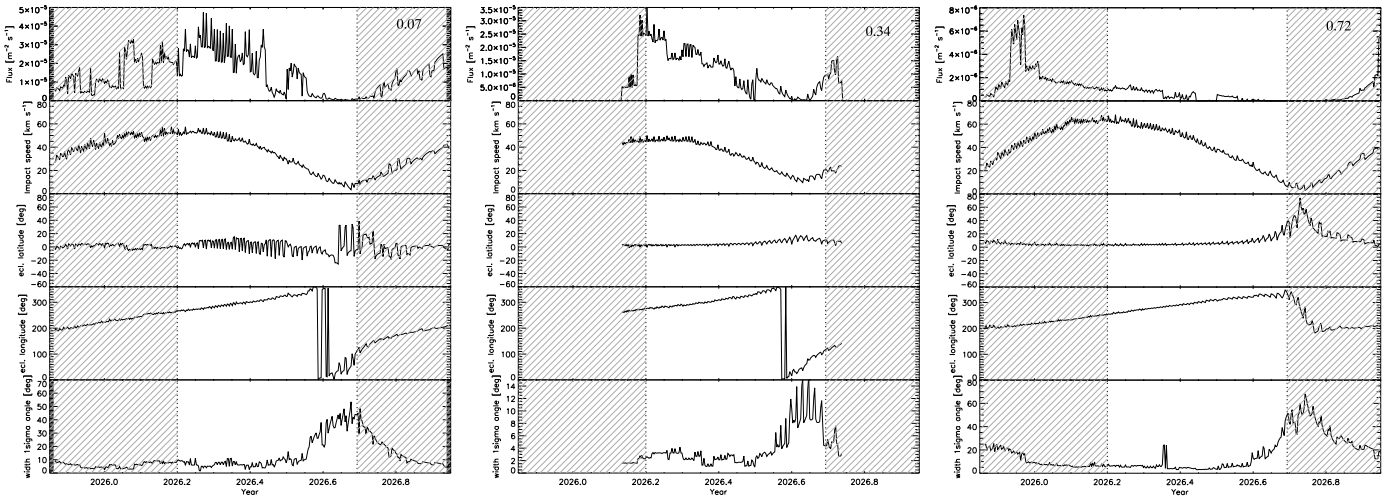

Fig. 7. Simulated impact rate, and dynamical parameters for particles with radius $r_d = 0.07$ μm (left column), 0.34 μm (middle column), 0.72 μm (right column) in the spacecraft reference frame during the Earth orbiting phase of DESTINY$^+$. Time intervals when interstellar dust particles will not be measurable based on the DDA Sun avoidance constraint are indicated by dashed areas. From top to bottom: impact rate, impact speed, impact direction of particles in ecliptic latitude β_{ecl} and ecliptic longitude λ_{ecl}, and the $1\,\sigma$ width of the interstellar dust flow. These quantities are averaged over all simulated particles hitting a grid cell of 0.25 AU side length. The time resolution along the spacecraft trajectory is 1/20 day.

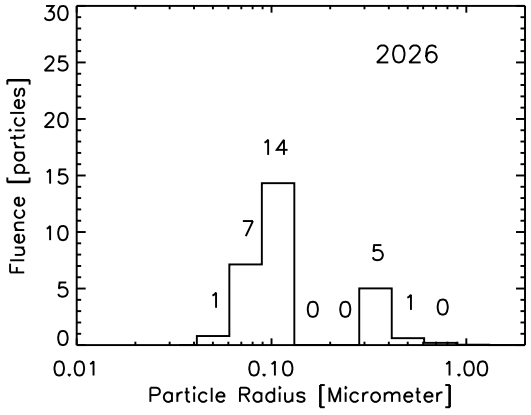

Fig. 8. Dust fluences for the Earth orbiting phase of DESTINY$^+$ for all relevant particle sizes, taking into account the DDA Sun pointing constraint (cf. Fig. 6).

The dust fluences for the individual particle sizes are shown in Fig. 12, top left panel and summarized in Table 1. In total, 53 particle detections are predicted for 2027. Most of these detections are predicted for the sizes approximately 0.1 μm and smaller, while only seven particle detections are predicted with approximately 0.4 to 0.5 μm radius.

4.2.2. Mission extension beyond Phaethon flyby

The interplanetary magnetic field presently undergoes one of its transitions from the defocussing to the focussing configuration for interstellar dust. The strongest focussing is expected for the first half of the 2030s (Strub et al., 2019). In order to study the detection conditions of DDA for interstellar dust in this time interval, we performed our simulations until the end of the available DESTINY$^+$ sample trajectory in 2032. In Fig. 4 this extended part covers the outermost portion of the DESTINY$^+$ trajectory. Here two revolutions of the spacecraft around the Sun are superimposed.

The dust fluxes for this extended mission phase are also shown in Fig. 10. The fluxes of the smallest particles below 0.1 μm significantly increase beginning in 2028 due to the increased focussing of the dust flow towards the ecliptic plane. It mostly affects the smallest particles due to their strong electromagnetic interaction with the IMF as compared to the bigger ones. Furthermore, the interstellar dust detections benefit from the larger heliocentric distance of DESTINY$^+$ where the filtering of particles with high β is weaker.

Table 1 shows that the yearly fluences increase by approximately a factor of three to four as compared to 2027. This leads to a total number of 160 to 190 detectable interstellar particles per year beginning in 2028, and a maximum of about 500 per year in 2030/31. It should be noted that these numbers are strongly dominated by the smallest particles below approximately 0.1 μm where we have the largest uncertainties in the model (Landgraf, 2000; Sterken et al., 2012; Strub et al., 2019).

Fig. 12 shows the size distributions for these time intervals. As pointed out before, very few particles with sizes of approximately 0.5 μm and bigger will be detectable. The vast majority of the detectable interstellar particles will be approximately 0.1 μm in size and smaller.

In 2032 the available DESTINY$^+$ trajectory covers only a fraction of the allowed detection window for interstellar dust which leads to a somewhat low fluence in that interval. The average impact rate, however, is even higher than in 2030/31 due to the continued focussing by the IMF.

4.3. Detection conditions for the spectral features of organic compounds

The measurements of the Cassini Cosmic Dust Analyzer at Enceladus have shown that spectral features of simple and more complex organics in the ice grains strongly depend on the particle impact speed and can be seen in impact spectra recorded below approximately 20 km s^{-1} (Kissel and Krueger, 2001; Goldsworthy et al., 2002, 2003; Burchell and Armes, 2011; Hillier et al., 2014; Fielding et al., 2015; Khawaja, 2017; Postberg et al., 2018; Khawaja et al., 2019, 2023) (see also Section 5). In order to estimate the expected number of particle impacts with good measurement conditions for organic compounds with DDA we have considered two impact speed ranges: average impact speed (1) up to 30 km s^{-1} and (2) up to 20 km s^{-1}, respectively. The numbers of predicted particle detections in these two speed ranges are summarized in Table 2.

It turns out that during the Earth orbiting phase and in the nominal mission, the expected number of impacts with speeds below 20 km s^{-1} is very small, only three particle detections are predicted. Our simulations show that the extended mission is essential to get a statistically meaningful number of interstellar particles with good measurement conditions for the spectral features of organic compounds. The situation is somewhat better if we assume a higher speed limit of 30 km s^{-1}, but

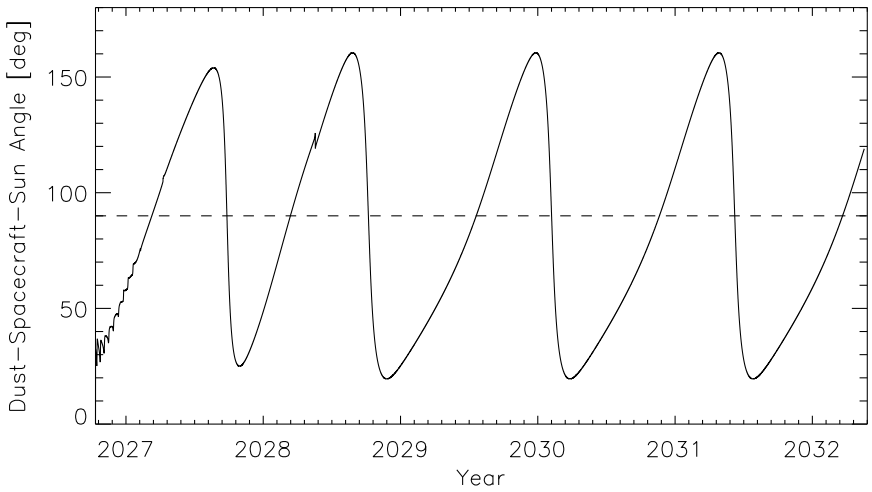

Fig. 9. Angle between the nominal interstellar dust direction and the direction towards the Sun in the spacecraft-centered reference frame during the interplanetary mission of DESTINY$^+$. Interstellar dust will not be measurable during the intervals when the angle is below 90° due to the DDA Sun avoidance constraint. In late 2026 and early 2027 the spacecraft is still in orbit around the Earth which leads to the wiggles, and the spike in May 2028 is due to a flyby at the Earth.

Table 1
Dust fluences and impact rates for the mission periods in Earth orbit and during the interplanetary mission which are allowed for interstellar dust measurements based on the DDA Sun avoidance constraint.

Mission phase	Time [yyyy-mm-dd]	Fluence	Impact Rate [day^{-1}]
Earth orbit	2026-03-14 to 2026-09-10	28	0.14
Nominal mission	2027-03-10 to 2027-09-25	54	0.24
Extended mission	2028-03-12 to 2028-10-05	162 (100[a])	1.09
	2029-07-19 to 2030-02-04	191	0.96
	2030-11-18 to 2031-06-06	519	2.60
	2032-03-19 to 2032-05-16[b]	191[b]	2.98

[a] Time interval from 2028-03-12 to the end of the nominal mission on 31 May 2028.
[b] This time interval covers the entire allowed detection window for interstellar dust in 2032 only partially due to the limited availability of DESTINY$^+$ trajectory data.

Table 2
Same as Table 1 but for two different ranges of the particle impact speed.

Mission Phase	Time [yyyy-mm-dd]	Fluence	Impact Rate [day^{-1}]
	$v < 20\,km\,s^{-1}$		
Earth orbit	2026-07-27 to 2026-09-10	1	0.02
Nominal mission	2027-07-31 to 2027-09-25	2	0.04
Extended mission	2028-08-07 to 2028-10-05	2	0.03
	2029-11-28 to 2030-02-04	9	0.13
	2031-04-09 to 2031-06-06	15	0.26
	$v < 30\,km\,s^{-1}$		
Earth orbit	2026-07-05 to 2026-09-10	2	0.03
Nominal mission	2027-07-09 to 2027-09-25	7	0.09
Extended mission	2028-07-16 to 2028-10-05	7	0.09
	2029-11-03 to 2030-02-04	27	0.29
	2031-03-21 to 2031-06-06	37	0.48

in this case a larger number of compounds will likely be destroyed during the impact process.

5. Discussion

Our simulations show that for the small particle sizes below approximately 0.1 μm the highest dust fluxes occur during approximately the first half of the time intervals allowed by the DDA Sun avoidance constraint (Figs. 6 and 10). Thus, interstellar dust measurements should preferentially be made during these intervals. The particle impact speeds are high in the range of 40 to 60 km s^{-1} in these periods which would allow for a distinction of interstellar from interplanetary dust if impact speeds can be determined with sufficient accuracy. DDA will measure the particle impact speeds with the trajectory sensor at the entrance of the instrument with approximately 10% accuracy which should be sufficient to distinguish interstellar from interplanetary particles (cf. Section 2 and Fig. 1), given that in the inner Solar System at approximately 1 AU heliocentric distance, the fluxes of interplanetary and interstellar dust are in the same range (Grün et al., 1997). It is additionally planned to constrain impact speeds by analyzing the recorded mass spectra, i.e. the occurrence of specific impact speed-dependent ion species (cf. Section 4.3).

During the second half of the intervals allowed by the DDA Sun avoidance constraint the speeds are significantly lower, which makes

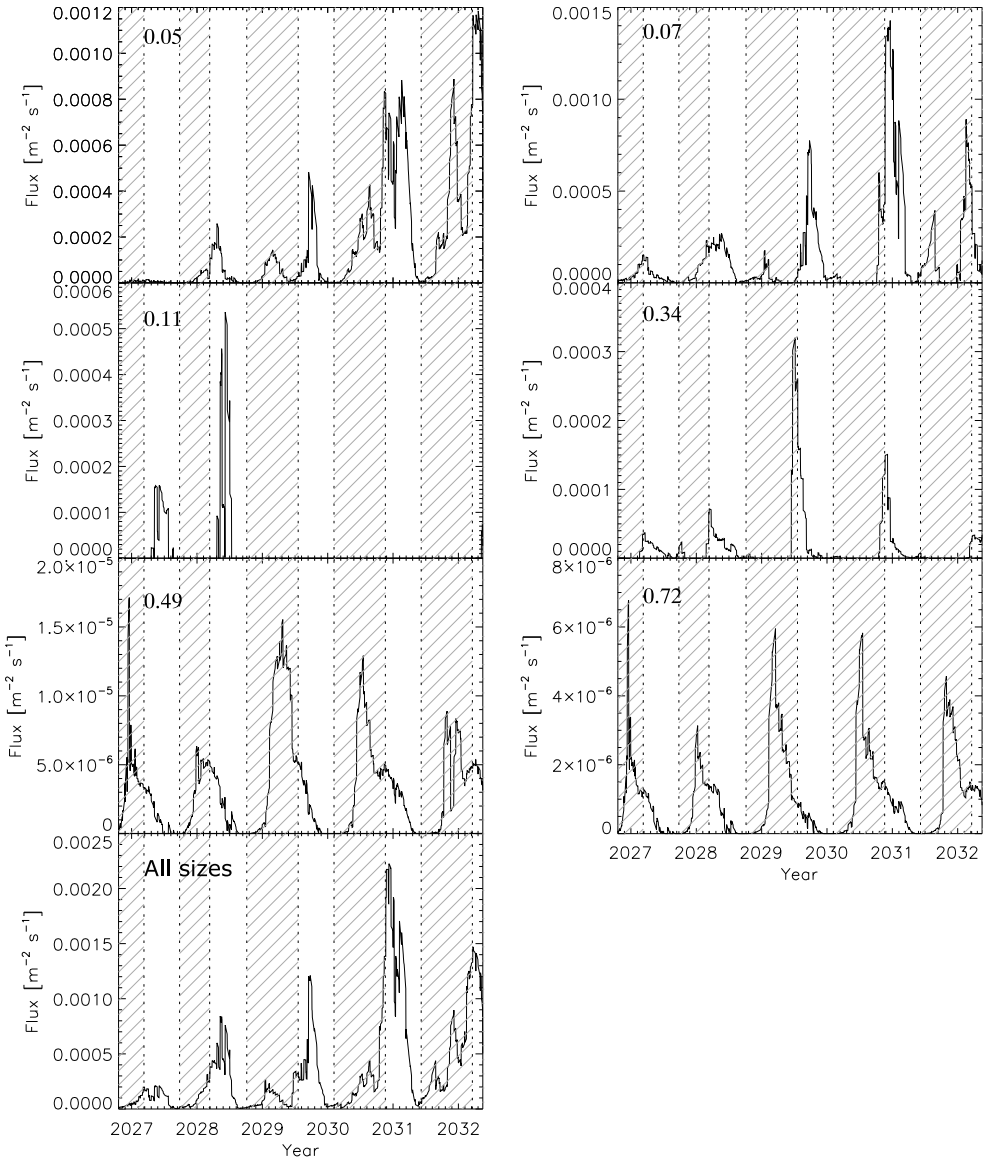

Fig. 10. Dust fluxes for the interplanetary mission of DESTINY$^+$ for all relevant particle sizes individually (top three rows) and for all sizes added together (bottom panel). The forbidden time intervals due to the DDA Sun avoidance constraint are indicated by the dashed areas. The time resolution along the spacecraft trajectory is 1 day. The numbers at the top left in each panel give the particle radius in micrometers.

the identification of interstellar particles by the speed ambiguous. On the other hand, these significantly lower speeds may open the possibility to analyze organic compounds in the particles which may be destroyed at higher impact speeds.

For the measurement of organic compounds, in addition to the impact speed, the degree of fragmentation (i.e. survivability) depends on the type of organics. Complex organic compounds, like hydrocarbon chains with aromatic structure and polyaromatic hydrocarbons, might show complex features above 100 u even above 20 km s^{-1}.

Between 15 and 25 km s^{-1} organic features occur in the mass range 26 to 31 u and probably also at 39 to 45 u (Srama et al., 2009; Hillier et al., 2014). If the organic material is complex and stable like Polycyclic Aromatic Hydrocarbons (PAHs) or Insoluble Organic Matter (IOM), complex spectral features might be observable above 50 u. Some impact experiments show spectral features at around 30 km s^{-1} that can be designated to organics between masses 26 to 31 u.

Major scientific questions related to interstellar dust are likely to be answered by DDA measurements: First, of major importance is a more precise evaluation of interstellar dust chemical composition, that can be addressed by the increased mass resolution of the DDA time-of-flight-mass spectrometer when compared to CDA (Altobelli et al., 2016; Simolka et al., 2024), and the here inferred higher number of measured particles, in particular during an extended mission of DESTINY$^+$. In particular, the upper limit of the fraction of chemically and isotopically anomalous circumstellar dust grains (Leitner et al., 2012) versus recondensed "ISM born" grains (Zhukovska et al., 2008) provides strong experimental constraints on models of the lifetime of interstellar dust, particularly time scales of destruction and recondensation, and models of cycling of grains between the various phases of the hot and cold interstellar medium (Trieloff et al., 2022). Another unresolved question related to the CDA measurements of interstellar dust by Altobelli et al. (2016) is an apparent deficit of volatile elements including carbon, which could be related to the loss of organic matter due to sublimation within the heliosphere (Kimura et al., 2020). In this context, measurements of interstellar dust particles impacting at low speed are particularly important in order to identify complex organic molecular fragments, which is possible during distinct time intervals identified in this study.

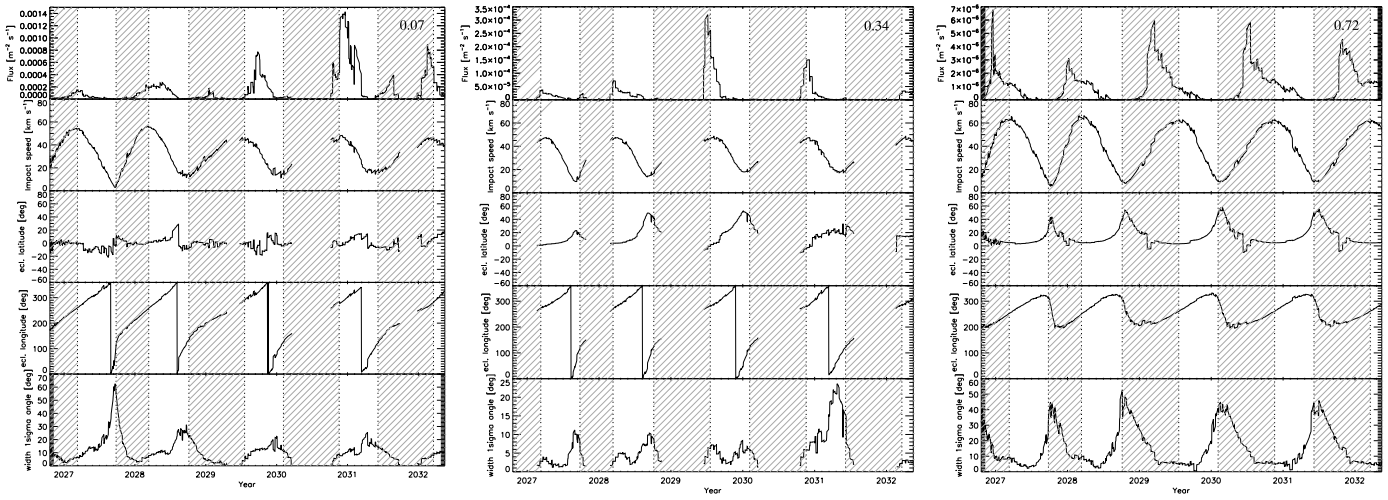

Fig. 11. Simulated impact rate, and dynamical parameters for particles with radius $r_d = 0.07$ μm (left column), 0.34 μm (middle column), 0.72 μm (right column) in the spacecraft reference frame during the interplanetary mission of DESTINY$^+$. Time intervals when interstellar dust particles will not be measurable based on the DDA Sun avoidance constraint are indicated by dashed areas. From top to bottom: impact rate, impact speed, impact direction of particles in ecliptic latitude β_{ecl} and ecliptic longitude λ_{ecl}, and the $1\,\sigma$ width of the interstellar dust flow. The time resolution along the spacecraft trajectory is 1 day.

Figs. 8 and 12 show that the relatively big interstellar particles exceeding approximately 0.5 μm in radius will remain basically undetectable for two reasons: (1) Based on the interstellar dust size distribution, their abundance significantly drops towards larger particle sizes, and (2) they are concentrated in the downstream direction behind the Sun where DDA cannot measure them due to its Sun avoidance constraint.

Interstellar particles in each size bin approach from a somewhat different direction because of their individual susceptibility to solar radiation pressure and the electromagnetic forces, and the DDA sensor orientation can be optimized for the expected approach direction of each particle size. Thus, the low detection number of big particles may be increased to some extent by pointing the DDA sensor towards the approach direction of these particles for some time. However, this leads to a reduced number of detections in the other size bins and in general a reduced overall dust fluence.

In order to investigate the significance of a DDA sensor pointing towards the approach direction of different sized particles, we have made IMEX simulations with an assumed DDA sensor pointing in the approach directions of the three particle sizes displayed in Figs. 7 and 11. When pointing the sensor towards the biggest particles (0.7 μm) the fluence of the particles with radius of approximately 0.5 μm is increased by about a factor of two, at the same time the fluence of the particles 0.3 μm and smaller is reduced by almost a factor of two. Thus, the total fluence is reduced by about 40%. The same is true if we optimize the sensor pointing for the 0.3 μm or the 0.07 μm particles: The fluence of these particles is increased by up to a factor of two but the total fluence is again reduced. This analysis shows that the largest overall fluence is obtained for a sensor pointing in the optimized sensor orientation as we have assumed throughout this paper.

The IMEX interstellar dust model has been calibrated with the Ulysses in situ dust measurements (Strub et al., 2019). In order to check the applicability of the model to other regions in space and time, we compared the modeled dust fluxes with the actual dust measurements obtained by other spacecraft (Galileo, Helios, Cassini; Krüger et al., 2019a). It showed that the model agrees with the measurements within a factor of 2 to 3. We expect that this accuracy is also valid for our predictions for DESTINY$^+$ presented in this work.

6. Summary

We used the IMEX interstellar dust model (Sterken et al., 2013; Strub et al., 2019) to predict dust fluxes and to study the dust detection conditions of the DESTINY$^+$ Dust Analyzer (DDA) on board the DESTINY$^+$ spacecraft which will be launched to the active asteroid (3200) Phaethon in 2025. We took into account the latest available spacecraft trajectory, the sensitivity profile of DDA, as well as the DDA Sun avoidance constraint.

Previously, CDA has reported on mass spectra for 36 submicrometer-sized interstellar dust particles. Our simulations show that due to the focussing configuration of the interplanetary magnetic field for interstellar dust which mostly affects the smallest particles below approximately 0.1 μm in radius, the fluences of such small particles significantly increase during the DESTINY$^+$ mission time. For the Earth orbiting phase of DESTINY$^+$ we predict that up to 28 interstellar particles will be detectable in 2026. For the interplanetary mission phase in 2027 this number increases to approximately 50 due to the increased focussing of interstellar dust by the interplanetary magnetic field. In 2028 and 2029/30 approximately 160 and 190 particles will be detectable, respectively, followed by a maximum of about 500 in 2030/31. The predicted impact rates of the particles are approximately 0.2 day^{-1} in 2026 and 2027, reaching 2.5 to 3.0 day^{-1} in the time interval 2030 to 2032. We believe that the uncertainty of these numbers is a factor of 2–3, based on a comparison of the predictions of the IMEX model with existing in situ spacecraft dust measurements (Krüger et al., 2019a).

As discussed above, the IMEX interstellar dust model has a systematic uncertainty of a factor of 2. We use this factor to calculate lower and upper limits to the model predictions. For the Earth orbiting phase in 2026, this gives a range of 14 … 56 particles, 25 … 100 particles in 2027, 80 … 320 in 2028, 95 … 380 particles in 2029/30, reaching a maximum of 250 … 1000 in 2030/31. While this uncertainty may seem large, the current understanding of the flow of interstellar dust is limited by the availability of data. To date, the Ulysses dust dataset that ended with the instrument's deactivation in 2007 is still the most comprehensive, homogeneous dataset for interstellar dust in the solar system. With DDA, a modern instrument will cover both the defocussing and focussing phases of interstellar dust, and provide valuable insights into the understanding of the dust flow and a foundation for improved models.

Interstellar particles larger than approximately 0.5 μm will most likely remain undetectable due to the interstellar dust size distribution which significantly drops towards large particle sizes. Furthermore, they are concentrated in the downstream direction behind the Sun where DDA cannot measure them due to its Sun avoidance constraint.

Measurements of interstellar dust particles impacting at low speed are particularly important in order to identify complex organic molecular fragments. This is possible during distinct time intervals identified

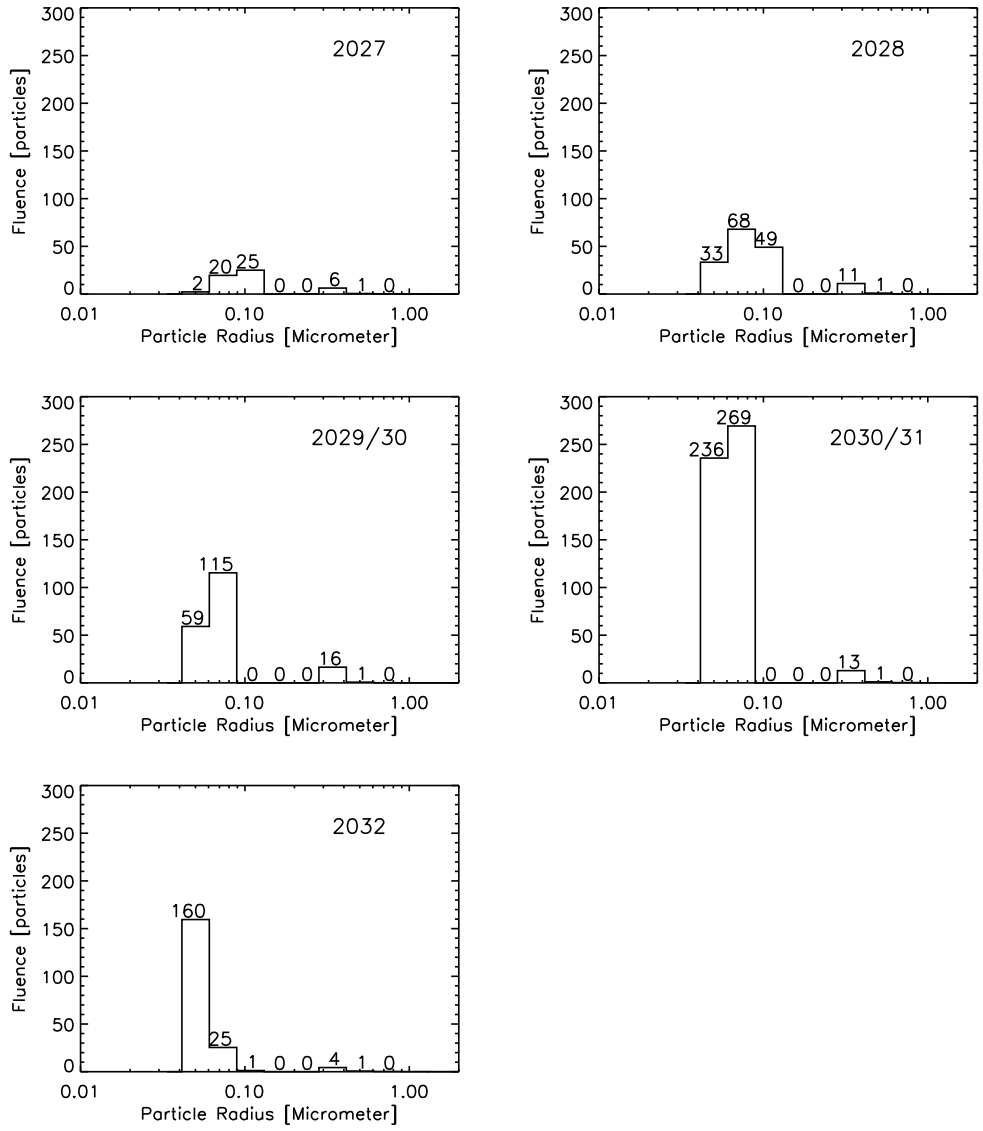

Fig. 12. Dust fluences for the interplanetary mission intervals when ISD will be detectable from 2027 to 2032 as given in Table 1 and Fig. 10. The numbers above each histogram bin give the number of particles detectable in that bin during that mission phase. *N* gives the total number of interstellar particles detectable during that mission period.

in this study. While organic compounds will be measurable only in a negligible number of particles during the Earth orbiting and the nominal interplanetary mission phases because of the low survivability of organics at impact speeds above about $20\,\mathrm{km\,s^{-1}}$, a statistically meaningful number of interstellar particle detections with measurable organic compounds is predicted for an extended mission after 2028.

The dust telescope DDA will measure the elemental, molecular and isotopic constituents of each detected dust particle with high mass resolution. In combination with its large sensor area and highly improved capabilities for measuring the particle trajectory in space it will open a new window for in situ dust analysis in space. A significantly higher particle detection statistics as compared to previous missions together with measurements over a wide range of impact speeds, in combination with the improved mass resolution, will provide new insights into the compositional diversity of the LIC particles. This will include grain formation and destruction processes as well as the significance of chemical processing of organic compounds in the interstellar medium.

CRediT authorship contribution statement

Harald Krüger: Writing – original draft, Supervision, Formal analysis. **Peter Strub:** Software, Investigation, Formal analysis. **Maximilian Sommer:** Writing – review & editing, Methodology. **Georg Moragas-Klostermeyer:** Software. **Veerle J. Sterken:** Software, Methodology. **Nozair Khawaja:** Methodology. **Mario Trieloff:** Writing – original draft, Methodology. **Hiroshi Kimura:** Writing – original draft, Methodology. **Takayuki Hirai:** Methodology. **Masanori Kobayashi:** Methodology. **Tomoko Arai:** Supervision, Methodology. **Jon Hillier:** Methodology. **Jonas Simolka:** Writing – original draft. **Ralf Srama:** Writing – original draft, Supervision.

Declaration of competing interest

The authors declare that they have no known competing financial interests or personal relationships that could have appeared to influence the work reported in this paper.

Acknowledgments

The IMEX model was developed under ESA funding (contract 4000106316/12/NL/AF - IMEX). Support by Deutsches Zentrum für Luft- und Raumfahrt, Germany (DLR, grant 50OO2101) and by MPS is also gratefully acknowledged. VJS received funding from the European Union's Horizon 2020 research and innovation programme under grant

agreement No. 851544 - ASTRODUST. We thank two anonymous referees whose comments improved the presentation of our results.

Data availability

No data was used for the research described in the article.

References

Altobelli, N., Postberg, F., Fiege, K., Trieloff, M., Kimura, H., Sterken, V.J., Hsu, H.W., Hillier, J., Khawaja, N., Moragas-Klostermeyer, G., Blum, J., Burton, M., Srama, R., Kempf, S., Gruen, E., 2016. Flux and composition of interstellar dust at saturn from Cassini's cosmic dust analyzer. Science 352, 312–318. http://dx.doi.org/10.1126/science.aac6397.

Arai, T., Kobayashi, M., Ishibashi, K., Yoshida, F., Kimura, H., Wada, K., Senshu, H., Yamada, M., Okudaira, O., Okamoto, T., Kameda, S., Srama, R., Krüger, H., Ishiguro, M., Yabuta, H., Nakamura, T., Watanabe, J., Ito, T., Ohtsuka, K., Tachibana, S., Mikouchi, T., Komatsu, M., Nakamura-Messenger, K., Sasaki, S., Hiroi, T., Abe, S., Urakawa, S., Hirata, N., Demura, H., Komatsu, G., Noguchi, T., Sekiguchi, T., Inamori, T., Yano, H., Yoshikawa, M., Ohtsubo, T., Okada, T., Iwata, T., Nishiyama, K., Toyota, H., Kawakatsu, Y., Takashima, T., 2018. Destiny^{+} mission: Flyby of geminids parent asteroid (3200) phaethon and in-situ analyses of dust accreting on the earth. In: Lunar and Planetary Institute Science Conference Abstracts. p. 2570.

Baalmann, L.R., Hunziker, S., Peronne, A., Kirchner, J.W., Glassmeier, K.H., Malaspina, D.M., Wilson, III, L.B., Strahl, C., Chadda, S., Sterken, V.J., 2024. A solar rotation signature in cosmic dust I: frequency analysis of dust particle impacts on the wind spacecraft. Astron. Astrophys. 689, A329. http://dx.doi.org/10.1051/0004-6361/20245006.

Baguhl, M., Grün, E., Hamilton, D.P., Linkert, G., Riemann, R., Staubach, P., 1995. The flux of interstellar dust observed by Ulysses and Galileo. Space Sci. Rev. 72, 471–476.

Baguhl, M., Grün, E., Linkert, G., Linkert, D., Siddique, N., 1993. Identification of 'small' dust impacts in the Ulysses dust detector data. Planet. Space Sci. 41, 1085–1098.

Battams, K., Knight, M.M., Kelley, M.S.P., Gallagher, B.M., Howard, R.A., Stenborg, G., 2020. Parker solar probe observations of a dust trail in the orbit of (3200) phaethon. Astrophys. J. Suppl. 246, 64. http://dx.doi.org/10.3847/1538-4365/ab6c68, arXiv:1912.08838.

Bertaux, J.L., Blamont, J.F., 1976. Possible evidence for penetration of interstellar dust into the solar system. Nature 262, 263–266.

Burchell, M.J., Armes, S.P., 2011. Impact ionisation spectra from hypervelocity impacts using aliphatic poly(methyl methacrylate) microparticle projectiles. Rapid Commun. Mass Spectrom. 25, 543–550. http://dx.doi.org/10.1002/rcm.4887.

Ceccarelli, C., 2023. Spiers memorial lecture: Astrochemistry at high resolution. Faraday Discuss. 245, 11–51. http://dx.doi.org/10.1039/D3FD00106G.

Cukier, W.Z., Szalay, J.R., 2023. Formation, structure, and detectability of the geminids meteoroid stream. Planet. Sci. J. 4, 109. http://dx.doi.org/10.3847/PSJ/acd538, arXiv:2306.11151.

Draine, B.T., Lee, H.M., 1984. Optical properties of interstellar graphite and silicate grains. Astrophys. J. 285, 89–108.

Fielding, L.A., Hillier, J.K., Burchell, M.J., Armes, S.P., 2015. Space science applications for conducting polymer particles: Synthetic mimics for cosmic dust and micrometeorites. Chem. Commun. 51, 16886–16899. http://dx.doi.org/10.1039/C5CC07405C.

Flandes, A., Krüger, H., Hamilton, D.P., Valdés-Galicia, J.F., Spilker, L., Caballero, R., 2011. Magnetic field modulated dust streams from Jupiter in interplanetary space. Planet. Space Sci..

Frisch, P.C., Dorschner, J., Geiß, J., Greenberg, J.M., Grün, E., Landgraf, M., Hoppe, P., Jones, A.P., Krätschmer, W., Linde, T.J., Morfill, G.E., Reach, W.T., Slavin, J., Svestka, J., Witt, A., Zank, G.P., 1999. Dust in the local interstellar wind. Astrophys. J. 525, 492–516.

Gail, H.P., Zhukovska, S.V., Hoppe, P., Trieloff, M., 2009. Stardust from asymptotic giant branch stars. Astrophys. J. 698, 1136–1154. http://dx.doi.org/10.1088/0004-637X/698/2/1136.

Godenko, E.A., Izmodenov, V.V., 2024. The unexpected role of heliospheric boundaries in facilitating interstellar dust penetration at 1-5 AU. Astron. Astrophys. 687, L4. http://dx.doi.org/10.1051/0004-6361/202450257.

Goldsworthy, B.J., Burchell, M.J., Cole, M.J., Armes, S.P., Khan, M.A., Lascelles, S.F., Green, S.F., McDonnell, J.A.M., Srama, R., Bigger, S.W., 2003. Time of flight mass spectra of ions in plasmas produced by hypervelocity impacts of organic and mineralogical microparticles on a cosmic dust analyser. Astron. Astrophys. 409, 1151–1167. http://dx.doi.org/10.1051/0004-6361:20031087.

Goldsworthy, B.J., Burchell, M.J., Cole, M.J., Green, S.F., Leese, M.R., McBride, N., McDonnell, J.A.M., Müller, M., Grün, E., Srama, R., Armes, S.P., Khan, M.A., 2002. Laboratory calibration of the cassini cosmic dust analyser (CDA) using new, low density projectiles. Adv. Space Res. 29, 1139–1144. http://dx.doi.org/10.1016/S0273-1177(02)00129-1.

Göller, J.R., Grün, E., 1989. Calibration of the Galileo/Ulysses dust detectors with different projectile materials and at varying impact angles. Planet. Space Sci. 37, 1197–1206.

Goode, W., Kempf, S., Schmidt, J., 2023. Mapping the surface composition of Europa with SUDA. Planet. Space Sci. 227, 105633. http://dx.doi.org/10.1016/j.pss.2023.105633.

Greenberg, J.M., 1989. The core-mantle model of interstellar grains and the cosmic dust connection. In: Allamandola, L.J., Tielens, A.G.G.M. (Eds.), Interstellar Dust. Cambridge University Press, pp. 345–355.

Greenberg, J.M., Hage, J.I., 1990. From interstellar dust to comets: A unification of observational constraints. Astrophys. J. 361, 260. http://dx.doi.org/10.1086/169191.

Grün, E., Fechtig, H., Hanner, M.S., Kissel, J., Lindblad, B.A., Linkert, D., Maas, D., Morfill, G.E., Zook, H.A., 1992a. The Galileo dust detector. Space Sci. Rev. 60, 317–340.

Grün, E., Fechtig, H., Kissel, J., Linkert, D., Maas, D., McDonnell, J.A.M., Morfill, G.E., Schwehm, G.H., Zook, H.A., Giese, R.H., 1992b. The ulysses dust experiment. Astron. Astrophys. Suppl. 92, 411–423.

Grün, E., Gustafson, B.E., Mann, I., Baguhl, M., Morfill, G.E., Staubach, P., Taylor, A., Zook, H.A., 1994. Interstellar dust in the heliosphere. Astron. Astrophys. 286, 915–924.

Grün, E., Krüger, H., Landgraf, M., 2001. Cosmic dust. In: Balogh, A., Marsden, R., Smith, E. (Eds.), The Heliosphere At Solar Minimum: The Ulysses Perspective. Springer Praxis., pp. 373–404.

Grün, E., Staubach, P., Baguhl, M., Hamilton, D.P., Zook, H.A., Dermott, S.F., Gustafson, B.A., Fechtig, H., Kissel, J., Linkert, D., Linkert, G., Srama, R., Hanner, M.S., Polanskey, C., Horányi, M., Lindblad, B.A., Mann, I., McDonnell, J.A.M., Morfill, G.E., Schwehm, G.H., 1997. South-north and radial traverses through the interplanetary dust cloud. Icarus 129, 270–288.

Grün, E., Zook, H.A., Baguhl, M., Balogh, A., Bame, S.J., Fechtig, H., Forsyth, R., Hanner, M.S., Horányi, M., Kissel, J., Lindblad, B.A., Linkert, D., Linkert, G., Mann, I., McDonnell, J.A.M., Morfill, G.E., Phillips, J.L., Polanskey, C., Schwehm, G.H., Siddique, N., Staubach, P., Svestka, J., Taylor, A., 1993. Discovery of Jovian dust streams and interstellar grains by the Ulysses spacecraft. Nature 362, 428–430.

Gustafson, B.A.S., Lederer, S.M., 1996. Interstellar grain flow through the solar wind cavity around 1992. In: Gustafson, B.A.S., Hanner, M.S. (Eds.), IAU Colloq. 150: Physics, Chemistry, and Dynamics of Interplanetary Dust. pp. 35–38.

Hanuš, J., Delbo', M., Vokrouhlický, D., Pravec, P., Emery, J.P., Alí-Lagoa, V., Bolin, B., Devogèle, M., Dyvig, R., Galád, A., Jedicke, R., Kornoš, L., Kušnirák, P., Licandro, J., Reddy, V., Rivet, J.P., Világi, J., Warner, B.D., 2016. Near-earth asteroid (3200) phaethon: Characterization of its orbit, spin state, and thermophysical parameters. Astron. Astrophys. 592, A34. http://dx.doi.org/10.1051/0004-6361/201628666.

Herbst, E., van Dishoeck, E.F., 2009. Complex organic interstellar molecules. Annu. Rev. Astron. Astrophys. 47, 427–480. http://dx.doi.org/10.1146/annurev-astro-082708-101654.

Hillier, J.K., Green, S.F., McBride, N., Altobelli, N., Postberg, F., Kempf, S., Schwanethal, J., Srama, R., McDonnell, J.A.M., Grün, E., 2007. Interplanetary dust detected by the Cassini CDA chemical analyser. Icarus 190, 643–654. http://dx.doi.org/10.1016/j.icarus.2007.03.024.

Hillier, J.K., Sternovsky, Z., Armes, S.P., Fielding, L.A., Postberg, F., Bugiel, S., Drake, K., Srama, R., Kearsley, A.T., Trieloff, M., 2014. Impact ionisation mass spectrometry of polypyrrole-coated pyrrhotite microparticles. Planet. Space Sci. 97, 9–22. http://dx.doi.org/10.1016/j.pss.2014.04.008.

Horányi, M., 1996. Charged dust dynamics in the solar system. Annu. Rev. Astron. Astrophys. 34, 383–418.

Hsieh, H.H., Jewitt, D., 2005. Search for activity in 3200 phaethon. Astrophys. J. 624, 1093–1096. http://dx.doi.org/10.1086/429250.

Ishibashi, K., Okamoto, T., Yamada, M., Okudaira, O., Hong, P., Suzaki, Y., Ohta, M., Miyabara, T., Ishimaru, T., Sato, S., Arai, T., Yoshida, F., Kagitani, M., Kameda, S., Takashima, T., 2024. Development status of DESTINY+ two onboard cameras for flyby imaging of (3200) phaethon. In: LPI Contributions. p. 1750.

Jewitt, D., Li, J., Agarwal, J., 2013. The dust tail of asteroid (3200) phaethon. Astrophys. J. Lett. 771, L36. http://dx.doi.org/10.1088/2041-8205/771/2/L36.

Jørgensen, J.K., Belloche, A., Garrod, R.T., 2020. Astrochemistry during the formation of stars. Annu. Rev. Astron. Astrophys. 58, 727–778. http://dx.doi.org/10.1146/annurev-astro-032620-021927, arXiv:2006.07071.

Kawakatsu, Y., Itawa, T., 2013. Destiny mission overview: a small satellite mission for deep space exploration technology demonstration. Adv. Astronaut. Sci. 146, 13, 12–585.

Kempf, S., Srama, R., Altobelli, N., Auer, S., Tschernjawski, V., Bradley, J., Burton, M.E., Helfert, S., Johnson, T.V., Krüger, H., Moragas-Klostermeyer, G., Grün, E., 2004. Cassini between Earth and asteroid belt: first in-situ charge measurements of interplanetary grains. Icarus 171, 317–335.

Khawaja, N., 2017. Organic Compounds in Saturn's E-Ring and Its Compositional Profile in the Vicinity of Rhea (Ph.D. thesis). University of Heidelberg, Germany.

Khawaja, N., O'Sullivan, T.R., Klenner, F., Sanchez, L.H., Hillier, J., 2023. Discriminating aromatic parent compounds and their derivative isomers in ice grains from enceladus and europa using a laboratory analogue for spaceborne mass spectrometers. Earth Space Sci. 10, e2022EA002807. http://dx.doi.org/10.1029/2022EA002807.

Khawaja, N., Postberg, F., Hillier, J., Klenner, F., Kempf, S., Nölle, L., Reviol, R., Zou, Z., Srama, R., 2019. Low-mass nitrogen-, oxygen-bearing, and aromatic compounds in Enceladean ice grains. Mon. Not. R. Astron. Soc. 489, 5231–5243. http://dx.doi.org/10.1093/mnras/stz2280.

Kimura, H., 2015. Interstellar dust in the local cloud surrounding the Sun. Mon. Not. R. Astron. Soc. 449, 2250–2258. http://dx.doi.org/10.1093/mnras/stv427.

Kimura, H., 2017. High radiation pressure on interstellar dust computed by light-scattering simulation on fluffy agglomerates of magnesium-silicate grains with metallic-iron inclusions. Astrophys. J. Lett. 839, L23. http://dx.doi.org/10.3847/2041-8213/aa6c2d.

Kimura, H., Kobayashi, M., Wada, K., Arai, T., Ishiguro, M., Hanayama, H., Ishibashi, K., Hirai, T., Yoshida, F., Hong, P., 2019. On the detection of an ejecta dust cloud around asteroid (3200) phaethon by the DESTINY$^+$ dust analyzer. I. Blackbody approximation. Planet. Space Sci. (submitted for publication).

Kimura, H., Mann, I., 1998. The electric charging of interstellar dust in the solar system and consequences for its dynamics. Astrophys. J. 499, 454–462. http://dx.doi.org/10.1086/305613.

Kimura, H., Mann, I., 1999. Radiation pressure on porous micrometeoroids. In: Baggaley, W.J., Porubcan, V. (Eds.), Meteroids 1998. Astronomical Institute of the Slovak Academy of Sciences, pp. 283–286.

Kimura, H., Mann, I., Jessberger, E.K., 2003. Composition, structure, and size distribution of dust in the local interstellar cloud. Astrophys. J. 583, 314–321. http://dx.doi.org/10.1086/345102.

Kimura, H., Ohtsuka, K., Kikuchi, S., Ohtsuki, K., Arai, T., Yoshida, F., Hirata, N., Senshu, H., Wada, K., Hirai, T., Hong, P.K., Kobayashi, M., Ishibashi, K., Yamada, M., Okamoto, T., 2022. Electrostatic dust ejection from asteroid (3200) Phaethon with the aid of mobile alkali ions at perihelion. Icarus 382, 115022. http://dx.doi.org/10.1016/j.icarus.2022.115022.

Kimura, H., Postberg, F., Altobelli, N., Trieloff, M., 2020. Organic matter in interstellar dust lost at the approach to the heliosphere. Exothermic chemical reactions of free radicals ignited by the Sun. Astron. Astrophys. 643, A50. http://dx.doi.org/10.1051/0004-6361/201526964, arXiv:2009.13757.

Kissel, J., 1986. The Giotto Particulate Impact Analyser. ESA Special Publication, pp. 67–83.

Kissel, J., Glasmachers, A., Grün, E., Henkel, H., Höfner, H., Haerendel, G., Hoerner, H.von., Hornung, K., Jessberger, E.K., Krueger, F.R., Möhlmann, D., Greenberg, J.M., Langevin, Y., Silén, J., Brownlee, D., Clark, B.C., Hanner, M.S., Hoerz, F., Sandford, S., Sekanina, Z., Tsou, P., Utterback, N.G., Zolensky, M.E., Heiss, C., 2003. The cometary and interstellar dust analyzer for comet wild 2. J. Geophys. Res. (Planets).

Kissel, J., Krueger, F.R., 2001. Time-of-flight mass spectrometric analysis of ion formation in hypervelocity impact of organic polymer microspheres: comparison with secondary ion mass spectrometry, mass spectrometry and laser mass spectrometry. Rapid Commun. Mass Spectrom. 15, 1713–1718. http://dx.doi.org/10.1002/rcm.431.

Kissel, J., Krueger, F.R., Silén, J., Clark, B.C., 2004. The cometary and interstellar dust analyzer at comet 81p/wild 2. Science 304, 1774–1776. http://dx.doi.org/10.1126/science.1098836.

Kobayashi, M., Srama, R., Krüger, H., Arai, T., Kimura, H., 2018. Destiny$^+$ dust analyser. In: Lunar and Planetary Institute Science Conference Abstracts. p. 2050.

Krueger, F.R., Werther, W., Kissel, J., R., S.E., 2004. Assignment of quinone derivatives as the main compound class composing 'interstellar' grains based on both polarity ions detected by the 'cometary and interstellar dust analyser' (CIDA) onboard the spacecraft STARDUST. Rapid Commun. Mass Spectrom. 18, 103–111. http://dx.doi.org/10.1002/rcm.1291.

Krüger, H., Strub, P., Altobelli, N., Sterken, V., Srama, R., Grün, E., 2019a. Interstellar dust in the solar system: model versus in-situ spacecraft data. Astron. Astrophys. 626, A37. http://dx.doi.org/10.1051/0004-6361/201834316.

Krüger, H., Strub, P., Srama, R., Kobayashi, M., Arai, T., Kimura, H., Moragas-Klostermeyer, G., Altobelli, N., Sterken, V., Agarwal, J., Sommer, M., Grün, E., 2019b. Modelling destiny$^+$ interplanetary and interstellar dust measurements en route to the active asteroid (3200) phaethon. Planet. Space Sci. 172. http://dx.doi.org/10.1016/j.pss.2019.04.005.

Krüger, H., Strub, P., Sterken, V.J., Grün, E., 2015. Sixteen years of ulysses interstellar dust measurements in the solar system: I. mass distribution and gas-to-dust mass ratio. Astrophys. J. 812, 139. http://dx.doi.org/10.1088/0004-637X/812/2/139.

Lallement, R., Bertaux, J.L., 2014. On the decades-long stability of the interstellar wind through the solar system. Astron. Astrophys. 565, A41. http://dx.doi.org/10.1051/0004-6361/201323216.

Landgraf, M., 2000. Modelling the motion and distribution of interstellar dust inside the heliosphere. J. Geophys. Res. 105 (A5), 10303–10316.

Landgraf, M., Augustsson, K., Grün, E., Gustafson, B.A.S., 1999. Deflection of the local interstellar dust flow by solar radiation pressure. Science 286, 2319–2322.

Landgraf, M., Krüger, H., Altobelli, N., Grün, E., 2003. Penetration of the heliosphere by the interstellar dust stream during solar maximum. J. Geophys. Res. 108, 1–5.

Leitner, J., Vollmer, C., Hoppe, P., Zipfel, J., 2012. Characterization of presolar material in the CR Chondrite northwest Africa 852. Astrophys. J. 745, 38. http://dx.doi.org/10.1088/0004-637X/745/1/38.

Li, J., Jewitt, D., 2013. Recurrent perihelion activity in (3200) phaethon. Astron. J. 145, 154. http://dx.doi.org/10.1088/0004-6256/145/6/154.

Licandro, J., Campins, H., Mothé-Diniz, T., Pinilla-Alonso, N., de León, J., 2007. The nature of comet-asteroid transition object (3200) phaethon. Astron. Astrophys. 461, 751–757. http://dx.doi.org/10.1051/0004-6361:20065833.

Linde, T.J., Gombosi, T.I., 2000. Interstellar dust filtration at the heliospheric interface. J. Geophys. Res. 105, 10411–10418. http://dx.doi.org/10.1029/1999JA900149.

MacLennan, E., Granvik, M., 2024. Thermal decomposition as the activity driver of near-Earth asteroid (3200) Phaethon. Nat. Astron. 8, 60–68. http://dx.doi.org/10.1038/s41550-023-02091-w, arXiv:2207.08968.

Mann, I., 2010. Interstellar dust in the solar system. Annu. Rev. Astron. Astrophys. 48, 173–203. http://dx.doi.org/10.1146/annurev-astro-081309-130846.

May, B.H., 2007. A Survey of Radial Velocities in the Zodiacal Dust Cloud (Ph.D. thesis. Ph.D. thesis). Imperial College of Science, Technology and Medicine London, U. K.

Mukai, T., 1981. On the charge distribution of interplanetary grains. Astron. Astrophys. 99, 1–6.

Ozaki, N., Yamamoto, T., Gonzalez-Franquesa, F., Gutierrez-Ramon, R., Pushparaj, N., Chikazawa, T., Tos, D.A.D., Çelik, O., Marmo, N., Kawakatsu, Y., Arai, T., Nishiyama, K., Takashima, T., 2022. Mission design of DESTINY+: Toward active asteroid (3200) phaethon and multiple small bodies. Acta Astronaut. 196, 42–56. http://dx.doi.org/10.1016/j.actaastro.2022.03.029.

Postberg, F., Khawaja, N., Abel, B., Choblet, G., Glein, C.R., Gudipati, M.S., Henderson, B.L., Hsu, H.W., Kempf, S., Klenner, F., Moragas-Klostermeyer, G., Magee, B., Nölle, L., Perry, M., Reviol, R., Schmidt, J., Srama, R., Stolz, F., Tobie, G., Trieloff, M., Waite, J.H., 2018. Macromolecular organic compounds from the depths of Enceladus. Nature 558, 564–568. http://dx.doi.org/10.1038/s41586-018-0246-4.

Rocha, W.R.M., van Dishoeck, E.F., Ressler, M.E., van Gelder, M.L., Slavicinska, K., Brunken, N.G.C., Linnartz, H., Ray, T.P., Beuther, H., Garatti, A.C.o., Geers, V., Kavanagh, P.J., Klaassen, P.D., Justannont, K., Chen, Y., Francis, L., Gieser, C., Perotti, G., Tychoniec, Ł., Barsony, M., Majumdar, L., le Gouellec, V.J.M., Chu, L.E.U., Lew, B.W.P., Henning, T., Wright, G., 2023. JWST observations of Young protoStars (JOYS+): Detection of icy complex organic molecules and ions. I. CH_4, SO_2, $HCOO^-$, OCN^-, H_2CO, HCOOH, CH_3CH_2OH, CH_3CHO, CH_3OCHO, CH_3COOH. http://dx.doi.org/10.48550/arXiv.2312.06834, arXiv e-prints, arXiv:2312.06834, arXiv:2312.06834.

Ryabova, G.O., Avdyushev, V.A., Williams, I.P., 2019. Asteroid (3200) Phaethon and the Geminid meteoroid stream complex. Mon. Not. R. Astron. Soc. 485, 3378–3385. http://dx.doi.org/10.1093/mnras/stz658.

Sandford, S.A., Allamandola, L.J., Tielens, A.G.G.M., Sellgren, K., Tapia, M., Pendleton, Y., 1991. The interstellar C-H stretching band near 3.4 microns: Constraints on the composition of organic material in the diffuse interstellar medium. Astrophys. J. 371, 607. http://dx.doi.org/10.1086/169925.

Senger, R., 2007. Data Handling and Evaluation for Autonomous Experiments in Interplanetary Missions (Ph.D. thesis). Munich University of Technology, Germany.

Simolka, J., Blanco, R., Ingerl, S., Krüger, H., Sommer, M., Srama, R., Strack, H., Wagner, C., Arai, T., Bauer, M., Fröhlich, P., Gläser, J., Gräßlin, M., Henselowsky, C., Hillier, J., Hirai, T., Ito, M., Kempf, S., Khawaja, N., Kimura, H., Klinkner, S., Kobayashi, M., Lengowski, M., Li, Y., Mocker, A., Moragas-Klostermeyer, G., Postberg, F., Rieth, F., Sasaki, S., Schmidt, J., Sterken, V.J., Sternovsky, Z., Strub, P., Trieloff, M., Szalay, J., Yabuta, H., 2024. The DESTINY+ dust analyser - A dust telescope for analysing cosmic dust dynamics and composition. Phil. Trans. R. Soc. A 382 (2273), 20230199. http://dx.doi.org/10.1098/rsta.2023.0199.

Slavin, J.D., Frisch, P.C., Müller, H.R., Heerikhuisen, J., Pogorelov, N.V., Reach, W.T., Zank, G., 2012. Trajectories and distribution of interstellar dust grains in the heliosphere. Astrophys. J. 760, 46. http://dx.doi.org/10.1088/0004-637X/760/1/46.

Srama, R., Ahrens, N., Auer, S., Bradley, M., Dikarev, V.V., Economou, T., Fechtig, H., Görlich, M., Grande, M., Graps, A.L., Grün, E., Havnes, O., Helfert, S., Horányi, M., Igenbergs, E., Jeßberger, E.K., Johnson, T.V., Kempf, S., Krivov, A.V., Krüger, H., Moragas-Klostermeyer, G., Lamy, P., Landgraf, M., Linkert, D., Linkert, G., Lura, F., Mocker-Ahlreep, A., McDonnell, J.A.M., Möhlmann, D., Morfill, G.E., Müller, M., Roy, M., Schäfer, G., Schlotzhauer, G.H., Schwehm, G.H., Spahn, F., Stübig, M., Svestka, J., Tschernjawski, V., Tuzzolino, A.J., Wäsch, R., Zook, H.A., 2004. The cassini cosmic dust analyzer. Space Sci. Rev. 114, 465–518.

Srama, R., Kempf, S., Moragas-Klostermeyer, G., Altobelli, N., Auer, S., Beckmann, U., Bugiel, S., Burton, M., Economou, T., Fechtig, H., Fiege, K., Green, S.F., Grande, M., Havnes, O., Hillier, J.K., Helfert, S., Horanyi, M., Hsu, S., Igenbergs, E., Jessberger, E.K., Johnson, T.V., Khalisi, E., Krüger, H., Matt, G., Mocker, A., Lamy, P., Linkert, G., Lura, F., Möhlmann, D., Morfill, G., Otto, K., Postberg, F., Roy, M., Schmidt, J., Schwehm, G.H., Spahn, F., Sterken, V., Svestka, J., Tschernjawski, V., Grün, E., Röser, H.P., 2011. The cosmic dust analyser onboard CASSINI: Ten years of discoveries. CEAS Space J. 2, 3–16. http://dx.doi.org/10.1007/s12567-011-0014-x.

Srama, R., Woiwode, W., Postberg, F., Armes, S.P., Fuji, S., Dupin, D., J., O., Sternovsky, Z., Kempf, S., Moragas-Klostermeyer, G., Mocker, A., Grün, E., 2009. Mass spectrometry of hyper-velocity impacts of organic micrograins. Rapid Commun. Mass Spectrom. 23, 3895–3906. http://dx.doi.org/10.1002/rcm.4318.

Sterken, V.J., Altobelli, N., Kempf, S., Krüger, H., Srama, R., Strub, P., Grün, E., 2013. The filtering of interstellar dust in the solar system. Astron. Astrophys. 552, A130. http://dx.doi.org/10.1051/0004-6361/201219609.

Sterken, V.J., Altobelli, N., Kempf, S., Schwehm, G., Srama, R., Grün, E., 2012. The flow of interstellar dust into the solar system. Astron. Astrophys. 538, A102. http://dx.doi.org/10.1051/0004-6361/201117119.

Sterken, V.J., Baalmann, L.R., Draine, B.T., Godenko, E., Herbst, K., Hsu, H.W., Hunziker, S., Izmodenov, V., Lallement, R., Slavin, J.D., 2022. Dust in and around the heliosphere and astrospheres. Space Sci. Rev. 218, 71. http://dx.doi.org/10.1007/s11214-022-00939-7.

Sterken, V.J., Strub, P., Krüger, H., von Steiger, R., Frisch, P., 2015. Sixteen years of ulysses interstellar dust measurements in the solar system: III. Simulations and data unveil new insights into local interstellar dust. Astrophys. J. 812, 141. http://dx.doi.org/10.1088/0004-637X/812/2/141.

Sterken, V.J., Westphal, A.J., N, A., D., M., P., F., 2019. Interstellar dust in the solar system. Space Sci. Rev. 215, 43. http://dx.doi.org/10.1007/s11214-019-0607-9.

Sternovsky, Z., Horanyi, M., Ayari, E., Kempf, S., Mikula, R., Hillier, J., Postberg, F., Srama, R., Szalay, J.R., 2022. Detecting and analyzing interstellar dust particles in the local interstellar cloud. In: AGU Fall Meeting Abstracts. SH45F–2392.

Strub, P., Krüger, H., Sterken, V.J., 2015. Sixteen years of ulysses interstellar dust measurements in the solar system: II. Fluctuations in the dust flow from the data. Astrophys. J. 812, 140. http://dx.doi.org/10.1088/0004-637X/812/2/140.

Strub, P., Sterken, V.J., Soja, R., Krüger, H., Grün, Srama, R., 2019. Heliospheric modulation of the interstellar dust flow on to Earth. Astron. Astrophys. 621, A54. http://dx.doi.org/10.1051/0004-6361/201832644.

Swaczyna, P., Bzowski, M., Heerikhuisen, J., Kubiak, M.A., Rahmanifard, F., Zirnstein, E.J., Fuselier, S.A., Galli, A., McComas, D.J., Möbius, E., Schwadron, N.A., 2023. Interstellar conditions deduced from interstellar neutral helium observed by IBEX and global heliosphere modeling. Astrophys. J. 953, 107, arXiv:2307.06694.

Szalay, J.R., Pokorny, P., Horányi, M., Janches, D., Sarantos, M., Srama, R., 2019. Impact ejecta environment of an eccentric asteroid: 3200 phaethon. Planet. Space Sci. 165, 194–204. http://dx.doi.org/10.1016/j.pss.2018.11.001.

Tielens, A.G.G.M., 1998. Interstellar depletions and the life cycle of interstellar dust. Astrophys. J. 499, 267–272. http://dx.doi.org/10.1086/305640.

Tielens, A.G.G.M., 2005. The Physics and Chemistry of the Interstellar Medium. Cambridge University Press, Cambridge, UK, ISBN: 0521826349.

Tielens, A.G.G.M., 2012. Chemical and physical properties of interstellar dust. In: Tuffs, R.J., Popescu, C.C. (Eds.), The Spectral Energy Distribution of Galaxies - SED 2011. pp. 72–81. http://dx.doi.org/10.1017/S1743921312008782.

Trieloff, M., Kimura, H., Postberg, F., Krüger, H., Strub, P., Leitner, J., Sterken, V., Hunziker, S., Hillier, J., Hirai, T., Yabuta, H., Ito, M., Khawaja, N., Schwarz, W.H., Ludwig, T., Schmitt, J., Sasaki, S., Arai, T., Kobayashi, M., Srama, R., 2022. Comparing meteoritic stardust with contemporary interstellar dust measured by cassini and destiny+ - constraining models of dust processing in the interstellar medium. In: European Planetary Science Congress. http://dx.doi.org/10.5194/epsc2022-961, EPSC2022–961.

Westphal, A.J., Stroud, R.M., Bechtel, H.A., Brenker, F.E., Butterworth, A.L., Flynn, G.J., Frank, D.R., Gainsforth, Z., Hillier, J.K., Postberg, F., Simionovici, A.S., Sterken, V.J., Nittler, L.R., Allen, C., Anderson, D., Ansari, A., Bajt, S., Bastien, R.K., Bassim, N., Bridges, J., Brownlee, D.E., Burchell, M., Burghammer, M., Changela, H., Cloetens, P., Davis, A.M., Doll, R., Floss, C., Grün, E., Heck, P.R., Hoppe, P., Hudson, B., Huth, J., Kearsley, A., King, A.J., Lai, B., Leitner, J., Lemelle, L., Leonard, A., Leroux, H., Lettieri, R., Marchant, W., Ogliore, R., Ong, W.J., Price, M.C., Sandford, S.A., Sans Tresseras, J.A., Schmitz, S., Schoonjans, T., Schreiber, K., Silversmit, G., Solé, V.A., Srama, R., Stadermann, F.J., Stephan, T., Stodolna, J., Sutton, S., Trieloff, M., Tsou, P., Tyliszczak, T., Vekemans, B., Vincze, L., Von Korff, J., Wordsworth, N., Zevin, D., Zolensky, M.E., 30714 Stardust@home dusters, 2014. Evidence for interstellar origin of seven dust particles collected by the stardust spacecraft. Science 345, 786–791. http://dx.doi.org/10.1126/science.1252496.

Witte, M., 2004. Kinetic parameters of interstellar neutral helium. Review of results obtained during one solar cycle with the Ulysses/GAS-instrument. Astron. Astrophys. 426, 835–844. http://dx.doi.org/10.1051/0004-6361:20035956.

Witte, M., Banaszkiewicz, H., Rosenbauer, H., 1996. Recent results on the parameters of interstellar helium from the Ulysses/GAS experiment. Space Sci. Rev. 78 (1/2), 289–296.

Witte, M., Banaszkiewicz, M., Rosenbauer, H., McMullin, D., 2004. Kinetic parameters of interstellar neutral helium: updated results from the Ulysses/GAS instrument. Adv. Space Res. 34, 61–65. http://dx.doi.org/10.1016/j.asr.2003.01.037.

Wood, B.E., Müller, H.R., Witte, M., 2015. Revisiting Ulysses observations of interstellar helium. Astrophys. J. 801, 62+. http://dx.doi.org/10.1088/0004-637X/801/1/62.

Yang, K., Schmidt, J., Feng, W., Liu, X., 2022. Distribution of dust ejected from the lunar surface into the Earth-Moon system. Astron. Astrophys. 659, A120, arXiv:2204.01040.

Ye, Q., Wiegert, P.A., Hui, M.T., 2018. In search of recent disruption of (3200) phaethon: Model implication and hubble space telescope search. Astrophys. J. Lett. 864, L9. http://dx.doi.org/10.3847/2041-8213/aada46.

Yoshida, F., Hayamizu, T., Miyashita, K., Watanabe, H., Yamamura, H., Akitaya, H., Asai, A., Fujiwara, Y., Goto, T., Hashimoto, G.L., Hatanaka, A., Horaguchi, T., Ida, M., Imamura, K., Isobe, K., Ishiguro, M., Kaizuka, N., Kasebe, H., Kawasaki, Y., Kim, T., Kitazaki, K., Manago, N., Matsumura, M., Matsushita, H., Matsuura, S., Nakamura, T., Nagata, T., Noda, H., Ogawa, M., Ohshima, O., Owada, M., Saitou, K., Tsumura, M., Ueyama, Y., Watanabe, H., Yamamoto, Yoshihara, H., Fujiwara, T., Haraguchi, M., Hayashi, H., Hitotsuda, T., Horikawa, T., Ishida, K., Ito, T., Jin, S., Kang, W., Katayama, T., Kawabata, K.S., Kawasaki, R., Kim, K., Kita, M., Kitazaki, N., Kurisu, H., Matsushima, M., Matsumi, C., Mihari, A., Naka, M., Nakaoka, T., Nishihama, R., Nishiyama, Y., Nukui, S., Oba, M., Okamoto, T., Omori, Y., Seo, J., Shirakawa, H., Sugino, T., Tani, Y., Takagaki, K., Ueda, Y., Urakawa, S., Watanabe, M., Yamashita, K., Yamashita, M., Sato, I., Murayama, S., Arai, T., Herald, D., Higuchi, A., 2023. Multi-chord observation of stellar occultation by the near-Earth asteroid (3200) phaethon on 2021 october 3 (UTC) with very high accuracy. Publ. Astron. Soc. Jpn. 75, 153–168. http://dx.doi.org/10.1093/pasj/psac096.

Zhang, Q., Battams, K., Ye, Q., Knight, M.M., Schmidt, C.A., 2023. Sodium brightening of (3200) phaethon near perihelion. Planet. Sci. J. 4, 70, arXiv:2303.17625.

Zhukovska, S., Gail, H.P., Trieloff, M., 2008. Evolution of interstellar dust and stardust in the solar neighbourhood. Astron. Astrophys. 479, 453–480, arXiv:0706.1155.

Zinner, E., 2014. Presolar grains. In: Davis, A.M. (Ed.), In: Meteorites and Cosmochemical Processes, vol. 1, pp. 181–213.

Zubko, E., Wada, K., 2023. Phase ratio in single-scattering dust particles: Implication to future DESTINY$^+$ study of asteroid (3200) phaethon. Icarus 404, 115652. http://dx.doi.org/10.1016/j.icarus.2023.115652.